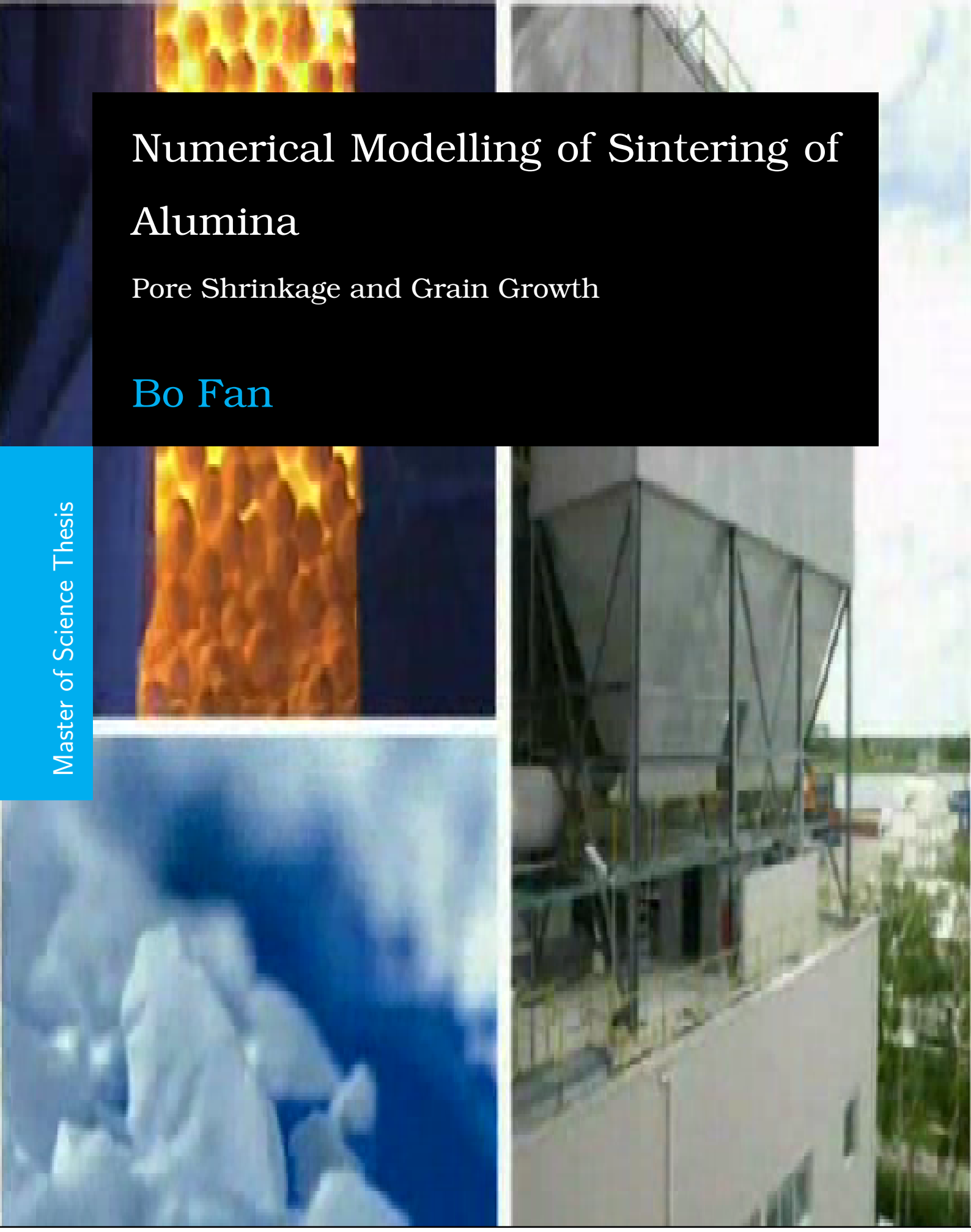

Numerical Modelling of Sintering of Alumina

Pore Shrinkage and Grain Growth

Bo Fan

Master of Science Thesis

TU Delft Delft University of Technology

Applied Mathematics

Numerical Modelling of Sintering of Alumina

Pore Shrinkage and Grain Growth

Master of Science Thesis

For the degree of Master of Science in Risk Analysis and Environmental Modelling at Delft University of Technology

Bo Fan

Student No. 4183762

August 26th, 2013

Department of Applied Mathematics (AM) · Faculty of Electrical Engineering, Mathematics and Computer Science (EEMCS) · Delft University of Technology (TUD)

The work in this thesis was supported by Almatis B.V.. Their cooperation is hereby gratefully acknowledged.

TU Delft Delft University of Technology

Delft University of Technology

Department of

AM

The undersigned hereby certify that they have read and recommend to the Faculty of EEMCS for acceptance a thesis entitled

Numerical Modelling of Sintering of Alumina

by

Bo Fan

in partial fulfillment of the requirements for the degree of

Master of Science Risk Analysis and Environmental Modelling

Dated: August 26th, 2013

Responsible Professor: _____

Prof. dr. ir. C. Vuik

Daily Supervisor: _____

Dr. Domenico Lahaye

Other Committee Member(s): _____

Mark van Dijk, Production Manager TAB, Almatis

_____

Dr. ir. W.T. van Horssen

Abstract

In this project we introduce the sintering process, which involves two basic phenomena, pore shrinkage and grain growth, occurring simultaneously. The objective of this project is to quantitatively describe the sintering process incorporating the kinetics of pore shrinkage and grain growth.

First we build a model for pore shrinkage separately. An important use of the results from pore shrinkage model is to estimate the relative density of the sintering material. Here we show an example with feedstock KA-13 in Ludwigshafen. The estimated result is reasonable, but not as good as expected, which means that lots of work are needed to be done in the future, such as more accurate measurements, adjustment of the model parameters and so on.

Using the same population balance equation as that used in the pore shrinkage model, we introduce the grain growth model, which only has different velocity model from that of pore shrinkage. Since during the intermediate stage of sintering, the kinetics of grain growth depends on the rate of pore shrinkage, we can further model the grain growth rate coupled with pore shrinkage through porosity or relative density, which depends on the solution of the pore shrinkage model.

Here we solve the PDEs using finite element method with COMSOL Multiphysics 4.3a (which is a software based on finite element method), and compare the results with analytical solution, solution generated using finite different method in Matlab. Initial values and parameters in the model are discussed as well. In the end we give an simple example with temperature cycle in the real system.

Acknowledgements

I would like to express my deep gratitude to Domenico Lahaye, my daily supervisor, for his patient guidance, enthusiastic encouragement and useful critiques of this project. Without his continued support during my graduation project, the work will not be accomplished so smoothly. I truly enjoyed our weekly inspiring discussions. I would also like to thank Prof. Kees Vuik, for his advice and assistance in keeping my progress on schedule.

I also want to acknowledge Almatis B.V. for providing such an opportunity. Especially thank Mark van Dijk and Wouter Zwijnenburg for sharing information in Almatis and their expertise.

In addition, I would like to thank Wim van Horssen for being my thesis committee member.

I would also like to extend my thanks to the Risk and Environmental Modeling group of TU Delft, for awarding me full scholarship for these two years' study. And thanks to all the teachers who used to teach me or help me in the past two years.

Last, but not least, I would like to thank my parents and my friends, for their endless support during my graduation project.

Bo Fan
Delft, University of Technology
August 24, 2013

Table of Contents

List of Figures

List of Tables

Chapter 1

Introduction

The objective of this project is to quantitatively describe the sintering process of alumina using numerical models. Since the process for the industrial production of alumina is not a familiar topic for most people, in the first chapter we'll introduce the basic properties of alumina and the whole process for production of alumina. Sintering is an important step during the whole production process of making premium alumina. In chapter 2, we explain the concept of sintering, discuss the quality control of sintering and introduce some important parameters in the sintering process. The early analytical model for solid state sintering process introduced in this chapter will help readers understand this process better. Chapter 3 - 5 are the most important parts in this thesis, especially chapter 3. In these three chapters, we introduce mathematical models for the sintering process, which includes two separate models and one combination model. All of these models are based on the number continuity equation. In chapter 3, using the pore shrinkage model we can get a reasonable estimation of the Dilato test result, which is useful in the quality control of sintering. In chapter 6, we try to use some temperature cycles which are closer to the reality to generate the model parameters and show the results. Chapter 7 is the conclusion part, where we discuss the results and the future work.

1-1 Alumina

Alumina is a chemical compound of aluminium and oxygen with the chemical formula Al_2O_3. It can be also called Aluminium oxide. This is a white or nearly colorless crystalline substance, as shown in Figure 1-1.

Figure 1-1: Alumina [3]

Alumina is a kind of widely known and used material for the production of aluminum. Besides, it's widely used for non-metallic applications. The key properties of alumina include [15]: high compression strength, high hardness, resistant to abrasion, resistant to chemical attack by a wide range of chemicals even at elevated temperature, high thermal conductivity, resistant to thermal shock, high degree of refractoriness, high dielectric strength, high electrical resistivity even at elevated temperatures, transparent to microwave radio frequencies, low neutron cross section capture area, and raw material readily available and so on. Due to its physical and chemical properties, alumina is playing an important role as an essential raw material for many market applications, such as ceramic, refractory, flame retardant polymer and etc..

1-2 Production of Alumina

1-2-1 Bayer Process

Generally, alumina can be got from bauxite, i.e. gibbsite ($Al(OH)_3$), boehmite ($AlO(OH)$) and diaspore ($AlO(OH)$). Deposits of bauxite ore are mined and refined into alumina. The most common method used to produce alumina is the Bayer process, which is invented in 1887 by Austrian scientist Karl Josef Bayer. There are also some other methods used in Russia and China. Details for these methods can be found in Luo.Z and Soria.A's report in 2007 [16]. Since Bayer process is the general method used for industrial production of alumina, here we use it as an example (See Figure 1-2) for better understanding of alumina production.

As shown in Figure 1-2, the process stages includes [17]:

- Wet Milling

  The bauxite is washed and crushed to increase its surface area. Lime and caustic soda (NaOH) are added.

- Digestion

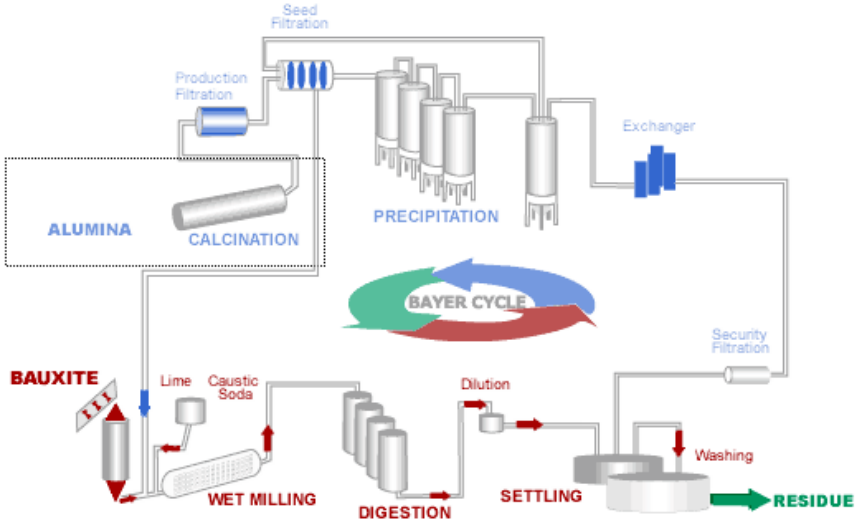

Figure 1-2: Bayer Process [4]

Hot caustic soda (NaOH) solution is used to dissolve the aluminium-bearing minerals in the bauxite to form a sodium aluminate supersaturated solution or "pregnant liquor".

Gibbsite: $Al(OH)_3 + Na^+ + OH^- \rightarrow Al(OH)_4^- + Na^+$

Boehmite, Diaspore: $AlO(OH) + Na^+ + OH^- + H_2O \rightarrow Al(OH)_4^- + Na^+$

- Settling

  The pregnant liquor got from digestion contains a solution of sodium aluminate and undissolved bauxite residues which contain iron, silicon and titanium. The slurry is flash cooled and an insoluble residue, known as red mud, is separated from the aluminate liquor via sedimentation. The bauxite residue sinks to the bottom of the settling tanks and then undergoes a series of washing stages to recover the caustic soda (which is reused in the digestion process).

  The purpose of the security filters is to ensure that the final product is not contaminated with impurities present in the residue.

- Precipitation

  The alumina is recovered by crystallisation from the pregnant liquor. The pregnant liquor is further cooled, resulting in the formation of small crystals of aluminium hydroxide ($Al(OH)_3$), which then grow and agglomerate to form larger crystals.

  $Al(OH)_4^- + Na^+ \rightarrow Al(OH)_3 + Na^+ + OH^-$

  This is an reverse of the reaction in the digestion stage.

- Calcination

  In the calciners temperature is up to 1100 °C. Free moisture and chemically-connected water are driven off. The following equation describes the calcination process.

  $2Al(OH)_3 \rightarrow Al_2O_3 + 3H_2O$

  Alumina solids is the final product of this step as well as the Bayer Process.

During the calcination process of aluminum hydroxides, many forms (crystalline phases) of alumina can be produced: α, χ, η, δ, κ, θ, γ, ρ [1].

Aluminum Hydroxide $Al(OH)_3 \rightarrow$ Transition Alumina $(\chi, \eta, \delta, \kappa, \theta, \gamma, \rho) \rightarrow \alpha - Al_20_3$

The common alumina phases can all be formed from room temperature up to about 1200 °C and end in the α phase (See Figure 1-3 [5]).

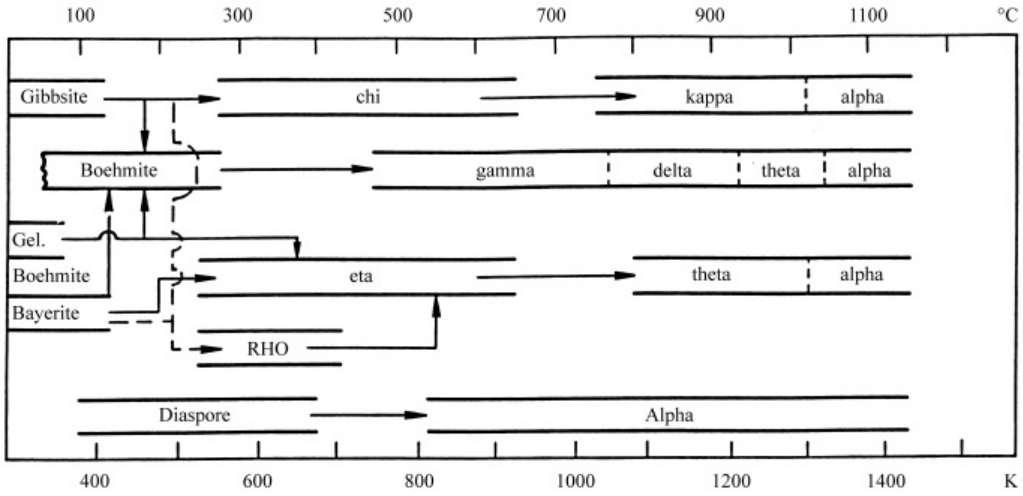

Figure 1-3: Thermal Transformation of Alumina Hydroxides [5]

If the alumina is not heated above 1200 °C, it'll adsorb water vapor very fast and no equilibrium was reached. Alumina produced in this period are called transition alumina. These are very complex materials. "Although the existence of the transition aluminas, specifically γ-, δ-, and θ- alumina, has been recognized for many years, their structure is still not well understood today. Lack of structural information is due in part to the growth characteristics of these forms of alumina. Large single crystals of these materials cannot be made, ..." - said by K.J. Morrissey [19].

[1] Use of Greek letters is common in chemistry to distinguish compounds with the same composition but different physical chemistry properties. For example, Jon Martin Andersson compared properties of three most important alumina phases α, θ, γ in 2005 [18]. These three alumina phases have different density.

Alumina heated above 1200 °C is called α-alumina by Rankin and Merwin [20]. This is the most thermal dynamically stable form of alumina. It has the same crystalline structure as the mineral corundum, as shown in Fig. 1-4.

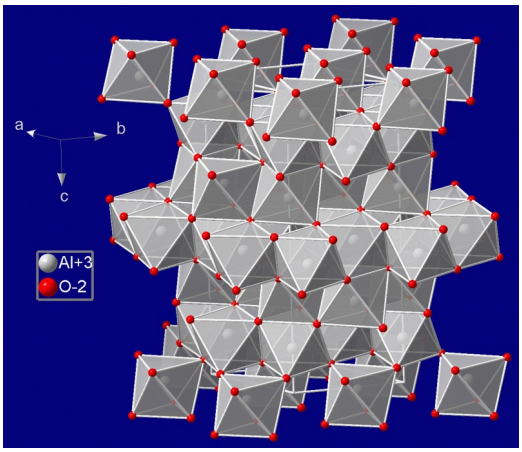

Figure 1-4: Crystal Structure of $\alpha - Al_2O_3$ [6]

During 1000-1250°C, the transformation from transition alumina to α-alumina is irreversible and it completes after a few hours more than 1250°C [21]. Above all, if a high enough temperature is used in the Bayer process for a long time, the final product is α-alumina, which is also called calcined alumina.

1-2-2 Tabular Alumina

During recent 70 years tabular alumina has been widely used in high performance refractory materials for many applications in steel, foundries petrochemistry and ceramics [22]. Tabular alumina derives its name from its morphology, which consists of large, 50-500μm, flat tablet-shaped crystals of corundum [15]. It can be produced by the sintering of calcined alumina.

The manufacture process of tabular alumina is shown in Figure 1-5, which includes the following steps [16]:

- Grinding: Make the fineness and surface of alumina satisfy a certain requirement in ball mill.
- Granulation: Make green balls[2] with grinding powder and water.
- Drying: Remove the moisture of the green balls. Too wet balls entering the converter will explode, because the water trapped inside the balls will become vapor as temperature increases. This mostly happens at the top of the converter.

[2]Green ball doesn't mean that the ball's colour is green. Here it is a relative concept to the sintered ball.

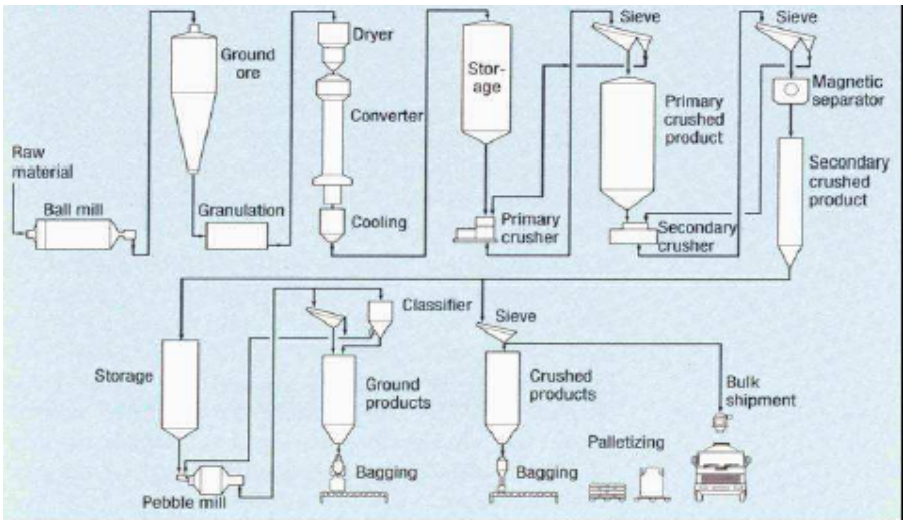

Figure 1-5: Production Process of Tabular Alumina by Sintering [7]

- Sintering: Send dried green balls to a vertical shaft kiln (converter), which is fired by a combination of nature gas and air. The sintering process is performed continuously at 1800-1900 °C, to obtain the highest mass density and lower porosity (see section 2-5-2). The powder particles recrystallize as hexagonal profile or even hexagonal prisms with $\alpha - Al_20_3$ structure [5]. The dried green balls are converted to tabular alumina.
- Crushing and sieving: Cool and crush the sintered converter discharge (CD) balls, sieve them to various opened and closed sized products.

In this project we only focus on the sintering process. The sintering process occurs above 1600°C and under α-alumina's melting point 2050°C in shaft kilns, which usually have gas burner in the median zone [23].

Chapter 2

Sintering of Alumina

What is sintering? Where does sintering take place? What happens during the sintering process? How can we control the quality of sintering? This chapter can help you better understand the above questions. First we give the definition of sintering process. Then we discuss about the driving force, mechanisms of sintering process and several approaches used in theoretical analysis of sintering. Details related to these topics are really a long story, so it's hard for us to explain all in this thesis. If readers want more information about this part, they can turn to the work of Kang [8] or M.N.Rahaman[1]. Here we just want to give readers a first impression of sintering process, which will be useful for better understanding of our model. In the end we discuss about quality control of sintering process and introduce some key parameters of sintering.

2-1 What is Sintering?

2-1-1 Definition and Driving Force of Sintering

Definition

Sintering is a processing technique used to produce density-controlled materials and components from metal or/and ceramic powders by applying thermal energy. When thermal energy is applied to a powder compact, the compact is densified and the average grain size increases [8].

Basically, sintering processes can be divided into two types: solid state sintering and liquid phase sintering. By Kang's definition [8]. "Solid state sintering occurs when the powder compact is densified wholly in a solid state at the sintering temperature, while liquid phase sintering occurs when a liquid phase is present in the powder compact during sintering".

To make our problem simple, here we only consider solid state sintering, since the melting point of aluminum oxide is generally 2050 °C and the temperature during the sintering process is below 2050 °C. In the real industry there might be also some other material, whose melting point is lower than 2050 °C, existing together with alumina. For example, generally, there might be some sodium oxide (Na_2O) left. And its melting point is around 1132 °C and boiling point is around 1950 °C. Then during the sintering process, the sodium oxide is in liquid phase. However, to make our problem simple in the beginning, we don't consider this situation, because except for alumina, other materials occupy relatively small percentage during the sintering of alumina. For example, the feedstock in Almatis contains 99.95% Al_2O_3.

Driving Force

The driving force of sintering process is the reduction in the total interfacial energy. The following formula (2-1) and figure (Figure 2-1) in Kang's book [8] explain this principle very well.

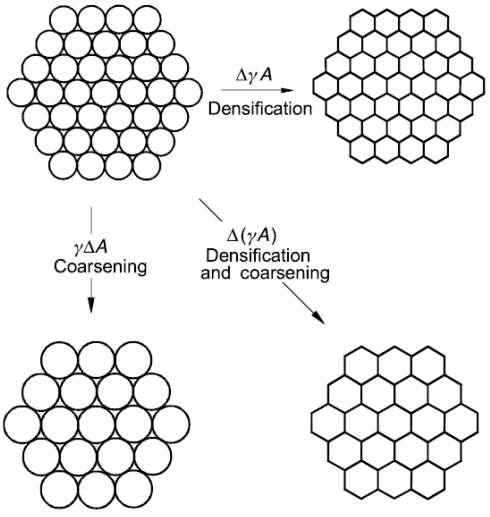

Figure 2-1: Basic Phenomena Occurs during Sintering [8]

"The total interfacial energy of a powder compact can be expressed as γA, where γ is the specific surface (interface) energy and A is the total surface (interface) area of the compact."

Then the change of total interfacial energy is

$$\Delta(\gamma A) = \gamma \Delta A + A \Delta \gamma \tag{2-1}$$

The change in interfacial energy ($\Delta\gamma$) is due to atom diffusion processes that lead to densification of the body (by transporting matter from inside the grains into the pores) and the change in total surface area (ΔA) is due to the atom diffusion processes that lead to coarsening of the microstructure (by rearrangement of matter between different parts of the pore surfaces without actually leading to a decrease in the pore volume). So the sintering process includes two processes: densification and coarsening. And it's necessary for us to understand the basic mass transport mechanism under the microstructure of particles and the relationship between these mechanisms and the two processes before building the model.

2-1-2 Mechanisms of Sintering

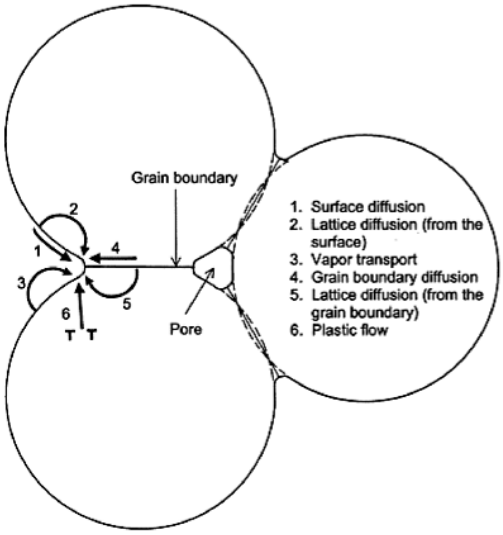

Figure 2-2: Transport Mechanisms [1]

There are at least 6 types of material transport mechanisms during sintering.

1 - Surface diffusion

"The free surface of a crystalline solid is not perfectly flat. It contains some vacancies (as in the bulk of the crystal), terraces, kinks, edges, and adatoms (See Figure 2-3). The migration of vacancies and the movement of adatoms provide the main mechanisms of surface diffusion." [1]

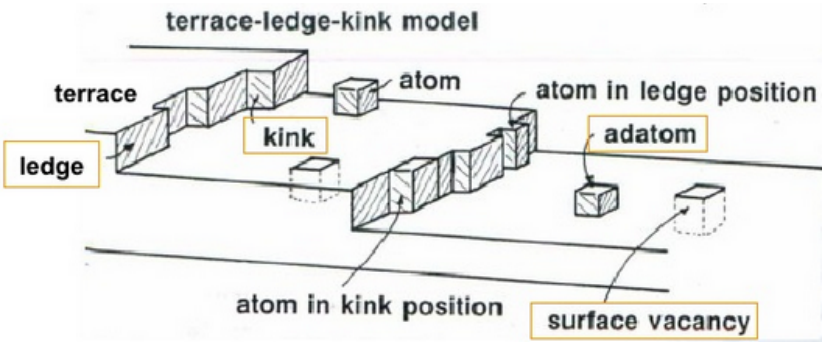

Figure 2-3: Solid Surface [1]

2,5 - Lattice [1] diffusion (volume diffusion or bulk diffusion)

Lattice diffusion takes place by the movement of point defects through the bulk of the lattice. The following figure (Fig. 2-4) shows the movement of atoms during lattice diffusion according to different mechanisms.

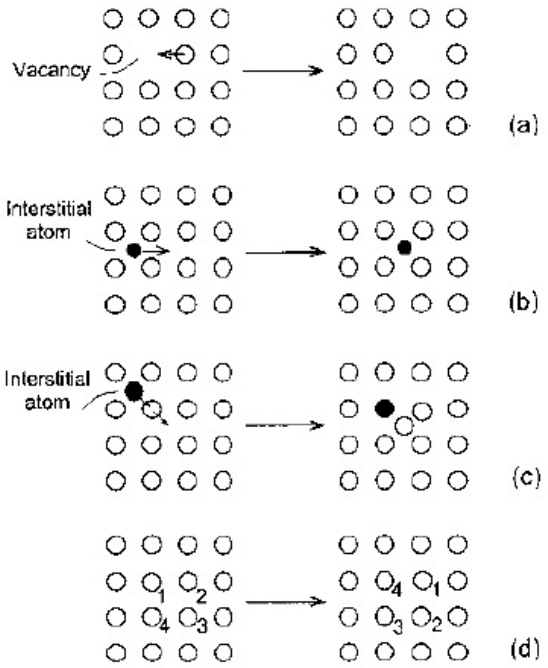

Figure 2-4: Lattice Diffusion [1]

3 - Vapor transport (evaporation-condensation)

Evaporation-condensation takes place because the vapour pressure on a curved surface is different from that on a flat surface or any other surface. The mass transport can proceed through a gas phase, driven by difference in vapour pressure. Atoms evaporate from the sphere surface

[1]Crystal lattice is a geometric arrangement of the points in space at which the atoms, molecules, or ions of a crystal occur.

and the evaporated atoms condense in the neck region [8]. For most materials, the evaporation-condensation transport is slow.

4 - Grain boundary diffusion

The grain boundary is usually assumed to be an area where no energy is required for atoms to attach or detach. The grains are separated from one another by grain boundaries, where lattice mismatch and disorder.

6 - Plastic flow

Plastic flow is the motion of dislocations under stress.

Details about these material transport mechanisms can be found in M.N.Rahaman's book [1]. In all of these mechanisms, the material transports from high chemical potential to low chemical potential. They all lead to bonding or neck growth between particles. We should notice that only certain mechanisms lead to pore shrinkage or densification. Surface diffusion, lattice diffusion (matter from the particle surfaces to the neck), and vapor transport lead to neck growth without densification and are referred to as nondensifying mechanisms. Grain boundary diffusion, lattice diffusion (matter from the grain boundary to the pore), and plastic flow are densifying mechanisms. The nondensifying mechanisms cannot simply be ignored because they reduce the driving force for sintering and so reduce the rate of the densifying mechanisms [1].

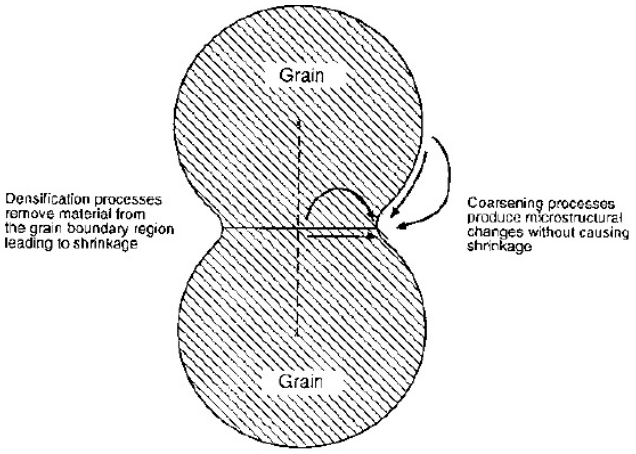

Figure 2-5: The Distinction between Densifying and Nondensifying Mechanisms [1]

Table 2-1: Mechanisms of Sintering

Mechanism	Source of matter	Sink of matter	Densifying or not
Surface diffusion	surface	neck	N
Lattice diffusion	surface	neck	N
Lattice diffusion	grain boundary	neck	Y
Grain boundary diffusion	grain boundary	neck	Y
Plastic flow	dislocations	neck	Y
Evaporation-condensation	surface	neck	N

2-2 Equipment Used for Sintering - Shaft Kilns (Converter)

Shaft kiln (converter, see Figure 2-6) is the equipment used for sintering process. It is operated by combustion of a mixture of natural gas and air and based on a very simple principle. The raw material (green ball) enters at the top of the kiln and the product is withdrawn from the bottom. The materials move slowly downwards through the kiln. Heat is added in the middle of the kiln. Therefore, materials above is preheated by rising hot exhaust gases and materials below is cooled by incoming air from the bottom. So the kiln can be divided into three operating sections: the pre-heating area, the burning area and the cooling area.

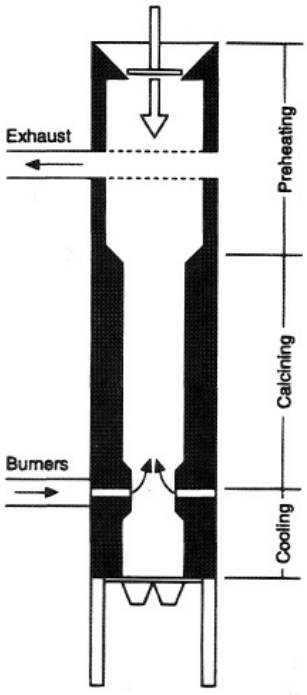

Figure 2-6: Shaft Kiln [9]

Figure 2-7 shows the temperature trajectory that the material goes through between entering and exiting the converter.

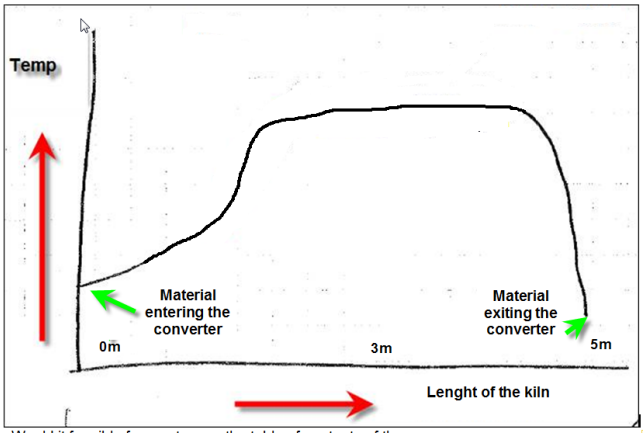

Figure 2-7: Sintering Process in the Shaft Kiln

Sintering temperature, heating and cooling rates are very important criteria for the quality of the products and are therefore strictly controlled.

2-3 Quality Control of Sintering

Optimization of an alumina sintering cycle is to achieve zero porosity (fully dense compact) with minimum possible grain growth. There are lots of items that would influence the final result, including both of the raw materials for sintering and the sintering environment.

Chemical composition of the powder compact will influence the sintering process. In industry field, 100% purify alumina doesn't exist. Generally, there are some other chemical composition included in the green ball. For example, the feedstock we used contains 99.95% Al_2O_3. There are also Fe_2O_3 (0.014%), SiO_2 (0.006%), TiO_2 (0.003%), Na_2O (0.360%), CaO (0.009%), Ga_2O_3 (0.011%), V_2O_5 (0.001%), ZnO (0.001%). Take Na_2O for example, the Sodium oxide's melting point is 1132 °C, while the general melting point for alumina is 2050 °C. It means that the liquid will exist at the sintering temperature and furthermore influence the sintering process. Besides, sodium oxide left in the CD balls will make the ball light yellow.

Partical size (also called grain size), partical shape, partical size distribution, degree of particle agglomeration of the green ball will also influence the sintering process further, since the raw material's density and densification time are related with these variables.

Insufficient control of temperature, time, atmosphere, pressure, heating and cooling rate in the shaft kiln will change the sintered microstructure, too. For example, if the balls travel too fast

in the converter, the crystallization won't complete and we'll get border balls with low density. If the ball travel too slow in the converter, the material will be melted a bit. This is bad for the grain growth and the density could also get down. If the temperature is too high, we could also have fusing in the converter then a large number of balls are fused together, like big lumps of material. In the worst case the converter itself can fuse together, then we really have a problem.

To observe the quality of sintering and to guarantee a stable product quality, we can get samples from the converter at fixed time point and see the microstructure of the fired balls. Figure 2-8 shows some examples of the crystal structure under microscope: We can see that

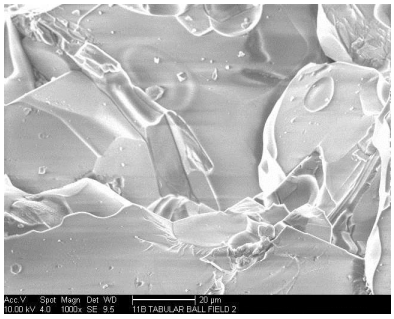

(a) Over fired, 1000x

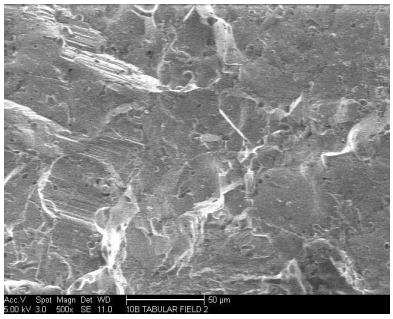

(b) Over fired with a bit fusing, 500x

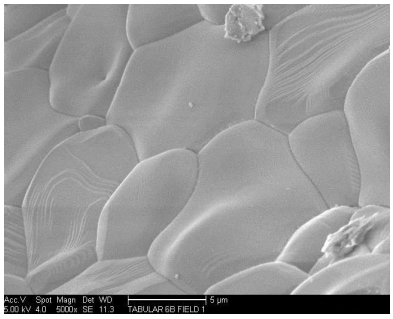

(c) Well fired, 5000x

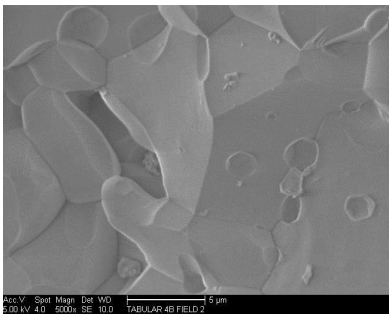

(d) OK, 5000x

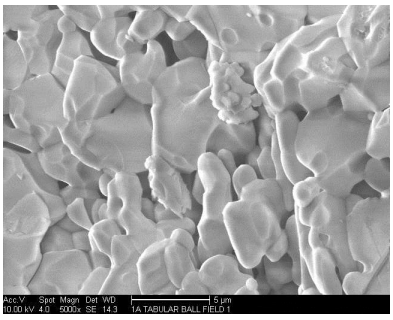

(e) Border, 5000x

Figure 2-8: Crystal Structure under Microscope

for the over fired ball, very large reflected crystals overlapping entire ball. Shape of crystals appear somewhat spherical. For the well fired ball, large reflected crystals overlapping entire ball. For the ball that is OK, fine reflected crystals not overlapping entire ball. For the border ball, there are white chalky marks in appearance with some sporadic reflected crystals.

Further quality control is carried out by the laboratory, monitoring both the chemical composition and the physical properties of the material, by the following characteristics: bulk specific gravity (B.S.G), apparent porosity and water absorption. Generally we can get B.S.G and temperature data under 1750°C in the lab with dried green balls (the dried green balls used in the lab and the balls we used in the real industrial process are the same). Then we hope to build a

mathematical model which describes the entire sintering process as well as the evolution of the microstructure (e.g. grain size, pore size, and the distribution of the grain and pore sizes), so that to help us control the sintering process. We can use existing experiment data to estimate parameters in the model and then try to estimate the situations in different temperature cycles, in order to improve the quality of sintering.

2-4 Main Approaches used in Theoretical Analysis of Sintering [1]

2-4-1 Analytical Models for Solid State Sintering Process

The solid state sintering is usually divided into three states: initial stage, intermediate stage and final stage.

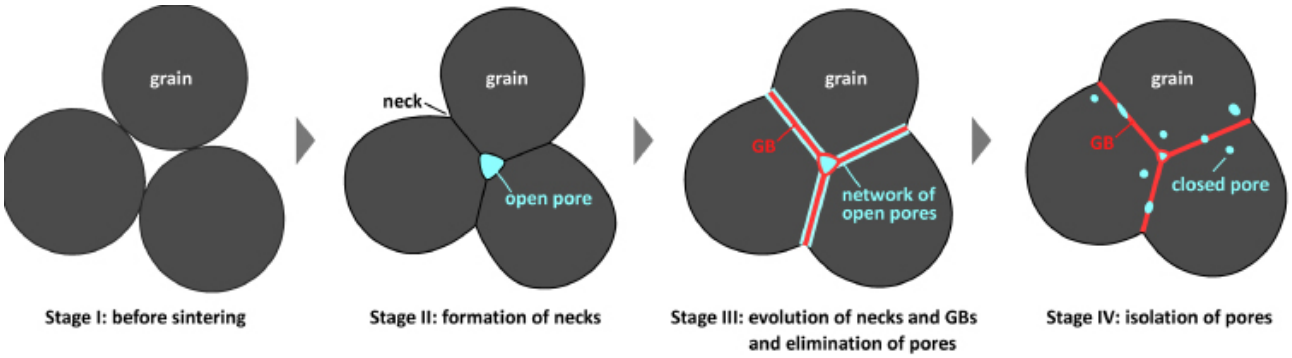

Figure 2-9: Three Stages of Solid State Sintering [10]

The initial stage is characterized by the neck formation between particles. During this stage, particles maintain their individual identity while neck growth takes place between them with relatively limited shrinkage of the compact.

During he intermediate stage, the particles lose their individual identity, pores become smooth and interconnect. Porosity is modeled as a network of interconnected channels running along the grain edges. Most of the densification and a great deal of grain growth occurs at this time. So this is the most important stage of sintering process.

In the final stage pores are isolated, grain growth is evident.

These analytical models help us understand the basis of sintering. Whereas these models assume an unrealistically simple geometry and often the occurrence of only a single mechanism, it's

Table 2-2: Stages of Sintering

Stage	Feature	Relative density rage	Model
Initial	neck formation	up to 0.65	two spheres in contact
Intermediate	continuous porosity	0.65 - 0.9	Tetrakaidecahedron with cylindrical pores along the edge
Final	isolated porosity	above 0.9	Tetrakaidecahedron with spherical pores at the corners

unsuitable for us to use these models for quantitatively predicting the sintering behavior of real powder systems. In fact, there are a lot of methods used in theoretical analysis of sintering.

2-4-2 Other Approaches

The development of the analytical models, is the first real attempt at a quantitative modeling of the sintering process. There are still lots of other approaches used to analyze sintering process (see Table 2-3).

Table 2-3: Approaches used for Theoretical Analysis of Sintering

Approach	Advantage	Disadvantage or Limitations
Analytical models	Useful for understanding basis of sintering	Too simple geometry; Based on single mechanism
Scaling laws	Useful for understanding the particle size dependence of the sintering mechanisms	Assume that particle size remains the same and the geometrical changes remain similar
Numerical simulations	Ability to analyze more realistic geometries	Require advanced numerical methods
Topological models	More appropriate to microstructural evolution	Predictions of kinetics limited
Statistical models	Simplified geometry	Semi-empirical analysis
Phenomenological equations	Empirical or phenomenological derivation of equations	No reasonable physical basis

The scaling laws [24], formulated at about the same time as the early analytical models, provide a guide for understanding the particle-size dependence of the sintering mechanisms. The topo-

logical models [25] make limited predictions of the sintering kinetics and are more appropriate to the understanding of the evolution of the microstructure. The statistical models [26] get little attention. The phenomenological equations are used to fit sintering data but add almost no insight into the process. Numerical simulations can analyze more realistic geometries than the analytical models as well as the occurrence of multiple mechanisms. Here we use the numerical analysis method.

2-5 Measurement of Sintering

To provide data for sintering kinetics, we need to measure the density or shrinkage of the powder compact at several times (or temperatures), and to give a plot of density or shrinkage versus sintering time (or temperature). Dilato test provides continuous monitoring of the linear shrinkage of the powder compact over the complete sintering schedule. Additional information from the microstructure, such as the pore size and pore size distribution, the grain size and grain size distribution, are also important to understand the sintering process.

2-5-1 Dilatometer test

Dilatometer test is a thermal analytical technique used to measure the expansion or shrinkage of solids, powders, pastes and liquids under negligible load when subjected to a controlled temperature/time program.

Dilatometer

Dilatometer is a scientific instrument that measures volume changes caused by a physical or chemical process. From the different kinds of dilatometers, we can get change of length, change of volume, relative change of length, linear thermal coefficient of expansion, differential thermal coefficient of expansion, volumetric thermal coefficient of expansion, softening point, transformation point, swelling behavior, penetration, shrinkage and change of density [27].

Principle of Dilatometer

Pushrod dilatometry is a method for determining dimensional changes versus temperature or time when temperature is changing overtime. Here is a simple example of dilatometer [11]:

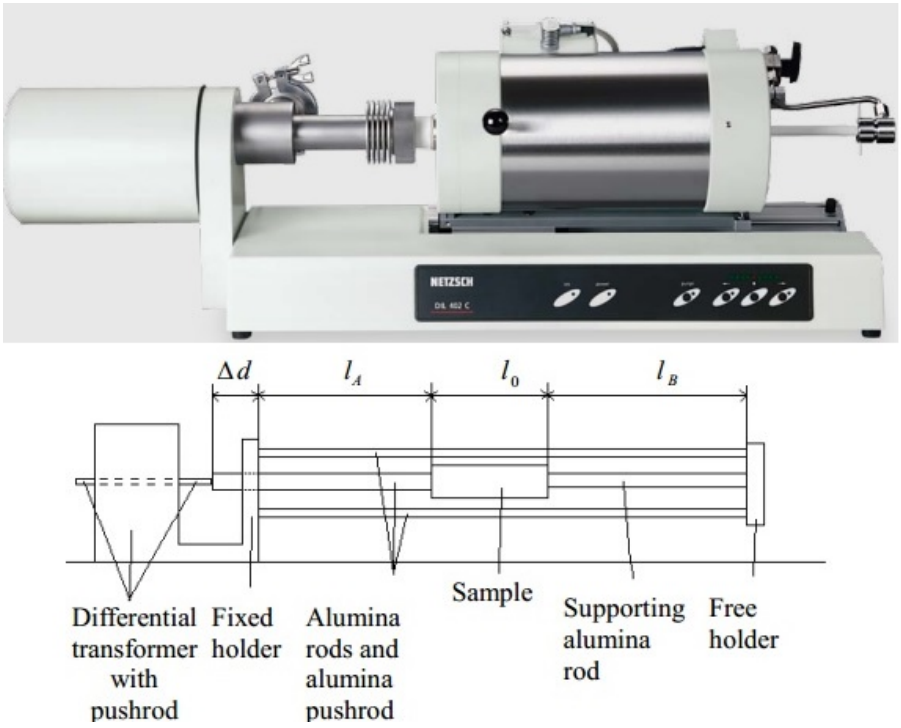

Figure 2-10: Dilatometer [11, 12]

We can measure the expansion of a known material (pushrod) and an unknown material (sample)[12]. In the parts l_A and l_B all rods expand to the right direction (because the left holder is fixed). The length of the sample l_0 is equal to the rod length l_c at the beginning of a measurement. At higher temperatures the rod expands to the right and also the unknown sample, but the sample has a different thermal expansion coefficient and it expands also to the left. We can estimate the expansion of the sample from Δl_c and $\Delta d = \Delta l_0 - \Delta l_c$, where Δl_0 is the expansion of sample and Δl_c is the expansion of rod.

$$\frac{\Delta l_0}{l_0} = \frac{\Delta l_c}{l_0} + \frac{\Delta d}{l_0} \tag{2-2}$$

The result of dilatometer test can be shown in Figure 2-11.

2-5-2 Pore Size and Pore Size Distribution

Pore

In fact, a completely accurate definition of a pore is almost impossible, because there are too many kinds of pores with different shapes and sizes. The shape of pores can be sphere, bubble-like, slip-shaped and so on. However, most pores' shapes are irregular and are changing over time. It can even not be described with dictionary words. In Dullien's book [13], pore is defined as "portion of pore space bounded by solid surfaces and by planes erected where the hydraulic

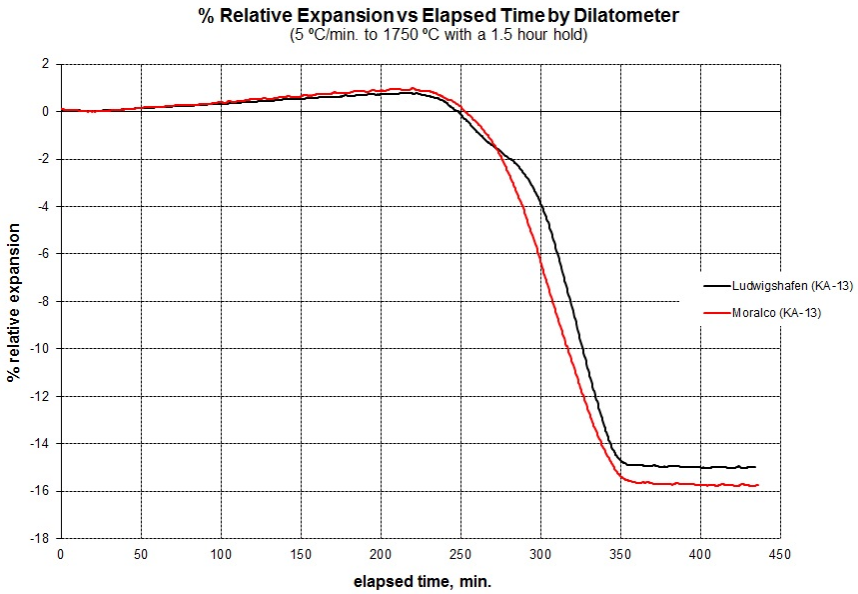

Figure 2-11: Dilatometer Test Result

radius of the pore space exhibits minima, analogously as a room is defined by its walls and the doors opening to it. If the local minima, the pore throats (the doors), can be located and imaginary partitions erected at these positions (the door closed) then the pores are defined, and their size can be determined by any arbitrary definition of size of an irregularly shaped object".

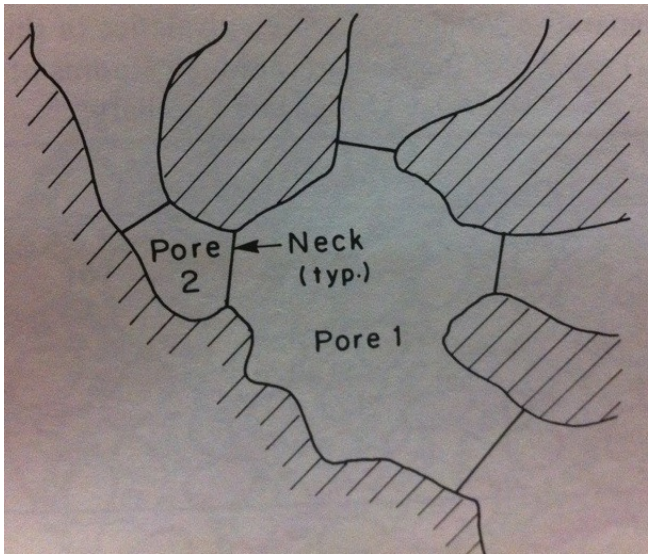

Figure 2-12: Pore [13]

The advantage of hydraulic radius is that it can be used to any shape of pores. The hydraulic radius $r_H = \frac{area\ \ of\ \ cross\ \ section}{length\ \ of\ \ perimeter\ \ of\ \ cross\ \ section}$.

Types of Pores

Open pore - forming a continuous phase within the medium.

Closed pore - non-interconnected/isolated pores that cannot contribute to the mass transport across the medium.

As shown in Figure 2-14, B is a closed pore and C is an open pore.

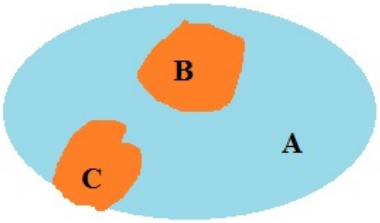

Figure 2-13: Open Pore and Closed Pore

Pore Size Distribution

For sphere shape, it's easy to define the size with it's radius or diameter. For aspheric shape, its maximum dimension, i.e. the greatest distance between any two surface points, has proven to be useful for characterizing size distributions [28].

The pore size distribution function n(r) (unit: $m^{-3}m^{-1}$) is defined such that n(r)dr is the total number of pores per unit volume of particles with sizes in the domain [r, r+dr]. The total number of particles is obtained by integrating n(r) over all sizes $\int_0^\infty n(r)dr$ (unit: m^{-3}).

According to Dullien and Batra's work [29], lots of methods for determining the pore size distribution are introduced. For example, mercury porosimetry (based on Archimedes' principle, see Appendix C), x-ray scattering, image analysis, etc... The widely used methods are mercury porosimetry (for macro range pores) and gas absorption (for meso range pores). But these two methods are only available for measuring open pores. Scanning electron microscopy (SEM) provides an image analysis method for us to measure the size of all pores. While enough pores must be included for statistic when image analysis method is used. From Jan Gerard Jacob Peelen's work [30] in 1977, the pore size distribution of sintered alumina fits log-normal distribution.

For the log-normal distribution, the representation of density function is as follows:

$$f(r) = \frac{1}{r^4\sqrt{2\pi}\ln\sigma} e^{-\frac{1}{2}(\frac{\ln r - \ln r_m}{\ln \sigma})^2} \tag{2-3}$$

This is defined by two parameters r_m and σ. r_m is geometric mean, and σ is geometric standard deviation.

$$\ln r_m = \frac{\Sigma((\ln r_i \Delta N_i))}{\Sigma \Delta N_i} \tag{2-4}$$

$$(\ln \sigma)^2 = \frac{\Sigma(\ln \frac{r_i}{r_m})^2 \Delta N_i}{\Sigma \Delta N_i} \tag{2-5}$$

Here N_i is the number of pores whose size are smaller than r_i. According to Charlie Zender's work [28] in 2010, r_m is the median radius of the log-normal distribution. And the geometry standard deviation is the ratio of the number of particles whose diameter are larger than 84.1% of all particles to the median diameter r_m.

2-5-3 Grain Size and Grain Size Distribution

Grain size and Grain size distribution will also influence the sintering process.

Grain (Particle) Size

For sphere shape, the diameter can be used to describe the grain size. For the irregular shape, size is hard to define. A simple way to define the size of an irregular shaped particle is the diameter of the sphere which has the same volume as the particle. But this method is not very helpful because in many cases it's hard to measure the volume of the particles. The particle size is usually defined arbitrarily by the measuring technique. The particle size measured by one technique may be quite different from that measured by another technique, even when the measuring instruments are operating properly.

In M.N.Rahaman's book [1], he mentioned several definitions of grain size. Surface diameter is the diameter of a sphere having the same surface area as the particle. Volume diameter is the diameter of a sphere having the same volume as the particle. Surface volume diameter is the diameter of a sphere having the same surface area to volume ratio as the particle. Stokes diameter (or equivalent spherical diameter) is the diameter of a sphere having the same sedimentation rate as the particle for laminar flow in a liquid. Projected area diameter is the diameter of a circle having the same area as the projected area of the particle. Perimeter diameter is the diameter of a circle having the same perimeter as the projected outline of the particle. Sieve diameter is the width of the minimum square hole through which the particle will pass. Feret's diameter is the mean value of the distance between pairs of parallel tangents to the projected outline of the particle.

Grain Size Distribution

M.N.Rahaman shows some common methods to measure the grain size distribution in his book (See Table 2-4)[1].

Table 2-4: Common Methods to Measure the Grain Size Distribution [1]

Method	**Measurement Range (μm)**
Microscopy	
Optical	>1
Scanning electron	>0.1
Transmission electron	>0.001
Sieving	20-10000
Sedimentation	0.1-100
Coulter counter	0.5-400
Light scattering	
Scattering intensity	0.1-1000
Brownian motion	0.005-1
X-ray line broadening	<0.1

Similar to the measurement of pore size, microscopy provides a straightforward method to measure the particle size and the individual shape of particles. Image analysis is necessary for this method and it needs a large number of particles within an appropriate size range on the image. Sieving is the oldest and one of the most widely used classification methods. However, it's time consuming and not available for powders where the particle size is less than 20 μm. It shouldn't be used for clean powders either since there might be some metallic impurities from the sieves. Sedimentation method is based on the Stoke's law (see Appendix D), so it's limited by the assumptions of Stoke's law such as "there are no collisions or interactions between the particles". Coulter counter is first applied to the counting of blood cells. In the coulter counter, the particles are suspended in electrolyte. The number and size of the particles are measured by causing them to flow through a narrow hole on either side of which an electrode is immersed. Particles passes through the hole will cause change in the electrical resistance, the magnitude of which is proportional to the volume of the particle. Light scattering method measures the particle size by measuring the scattering angle of light. And X-ray broadening method measures the particle size by measuring the width of the diffraction peak (or the size of the diffraction spot). This method gives a measure of the particle size regardless of whether

the particles consist of single crystals, polycrystal, or agglomerates.

From Tsung-shou Yeh and Michael D.Sacks' work [31] using X-ray sedimentation, the grain size distribution for alumina fits log-normal distribution. So the pore size distribution and grain size distribution we used in this project are both log-normal distributions. The advantage of log-normal distribution is that the shape of the distribution is unchanged for all moments. Thus, if the number distribution is log-normal, the surface and mass distributions will also be log-normal.

2-5-4 Density, Porosity, Water Absorption and Specific Gravity

Density

Density is the mass per unit volume, $\rho = \frac{m}{V}$;

Bulk Density $= \frac{Mass}{Bulk\ Volume\ (Total\ Volume)}$

$= \frac{Mass}{Solid\ Volume\ (A,\ True\ Volume)\ +Open\ Pore\ Volume\ (C)\ +\ Closed\ Pore\ Volume\ (B)}$

Apparent Density $= \frac{Mass}{Apparent\ Volume} = \frac{Mass}{Solid\ Volume\ +\ Closed\ Pore\ Volume\ (B)}$

True Density $= \frac{Mass}{True\ Volume} = \frac{Mass}{Solid\ Volume\ (A)}$

Theoretical Density $= \frac{Mass\ of\ a\ unit\ cell}{Volume\ of\ a\ unit\ cell}$

Porosity

Porosity is the fraction of the bulk volume of the porous sample that is occupied by pore or void space [13].

Apparent Porosity (AP) $= \frac{Open\ Pore\ Volume\ (C)}{Total\ Volume\ (A+B+C)} * 100\%$

True Porosity (TP) $= \frac{Total\ Pore\ Volume\ (B+C)}{Total\ Volume\ (A+B+C)} * 100\%$

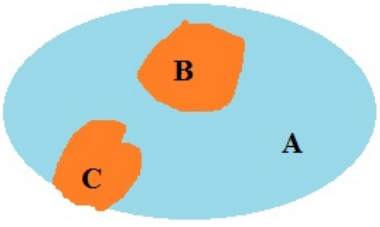

Figure 2-14: Open Pore and Closed Pore

Water Absorption

$$\text{Water Absorption (WA)} = \frac{Weight\ of\ Dry\ Piece\ Soaked\ in\ Fluid - Weight\ of\ Dry\ Piece\ in\ Fluid}{Weight\ of\ Dry\ Piece\ in\ Fluid} * 100\%$$

Specific Gravity

Specific Gravity (SG), or relative density, is the ratio of the density of a substance to the density of a given reference material [32, 33]. It is common to use the density of water at 4 °C (39 °F) as the reference material, because the density of water is highest at this point ($0.999972 g/cm^3$).

$SG = \frac{\rho_{sample}}{\rho_{H_2O}} = \frac{m_{sample}/V}{m_{H_2O}/V} = \frac{m_{sample}g}{m_{H_2O}g} = \frac{W_{sample}}{W_{H_2O}}$.

where ρ represents the density, m represents the mass, V represents the volume, W represents the weight and g is gravity of earth.

Bulk specific gravity (BSG) denotes specific gravity measurements in which volume of the substance includes both open and closed pores. Apparent specific gravity is used to denote the specific gravity of a porous solid when the volume used in the calculations is considered to exclude the open pores.

In the following chapters, when we mention about relative density or BSG, it's

$$\rho_r = \frac{Bulk \quad Density}{True \quad Density} = 1 - True \quad Porosity \tag{2-6}$$

Chapter 3

Model of Pore Shrinkage

There are a lot of models for simulating sintering process. In this project we introduce a mathematical model of sintering based on the combination of two general population balance model - one is for separate pore shrinkage process (see Chapter 3) and the other is for grain growth [1] (see Chapter 4). These two models are very similar, they only differ in the choice of velocity model. We use COMSOL Multiphysics 4.3a (which is an engineering, design, and finite element analysis software environment for the modeling and simulation of any physics-based system) to solve these problems and compare the result with analytical solution and matlab solution. In Chapter 5, we combine these two models together.

The most important thing in this chapter is that we can use the result of pore shrinkage model to calculate the relative density.

3-1 Particle-Number Continuity Equation

The continuity equation describes the transport of a conserved quantity, such as mass, energy, momentum and electric charge. A variety of physical phenomena may be described using continuity equations. The particle number continuity equation, or population balance equation is given by Randolph and Larson [34] as follows:

$$\frac{\partial n}{\partial t} + \nabla \cdot v_e n + \nabla \cdot v_i n + D - B = 0 \tag{3-1}$$

[1] Grain growth describes the increase in the grain size. While coarsening we mentioned in last chapter is used to describe the process of grain growth coupled with pore growth.

- n - number density function, defined in an (m+3)-dimensional space consisted of 3 external (spatial) coordinates and m internal coordinates (size, age and etc.)
- t - time
- v_e - external (spatial) particle velocity
- v_i - internal particle velocity
- D - particle death function
- B - particle birth function

This equation comes from the basic principle: in a fixed region

$$Accumulation = Input - Output + Net\ Generation \tag{3-2}$$

If we consider a fixed region R_1 with the convection velocity v ($v = v_e + v_i$),

$$\frac{d}{dt}\int_{R_1} ndR = \int_{R_1} (B - D)dR \tag{3-3}$$

Since

$$\frac{d}{dt}\int_{R_1} ndR = \int_{R_1} \frac{\partial n}{\partial t}dR + (nv)\mid_{R_1} = \int_{R_1} [\frac{\partial n}{\partial t} + \nabla \cdot (nv)]dR \tag{3-4}$$

$$\int_{R_1} [\frac{\partial n}{\partial t} + \nabla \cdot (nv) - B + D]dR = 0 \tag{3-5}$$

R_1 is chosen arbitrary, so

$$\frac{\partial n}{\partial t} + \nabla \cdot (nv) - B + D = 0 \tag{3-6}$$

$$\Rightarrow \frac{\partial n}{\partial t} + \nabla \cdot (v_e n) + \nabla \cdot (v_i n) - B + D = 0 \tag{3-7}$$

In our project, we use the number continuity equation for pore shrinkage as well as grain growth. To simplify the problem, we assume that:

(1) The sample is spatially homogeneous and sintering is a convectionless batch process, i.e. $v_e = 0$ [35];

(2) Sintering is coalescence free, i.e. $B - D = 0$ [35];

Then our the popular balance equation is simplified to:

$$\frac{\partial n}{\partial t} + \nabla \cdot v_i n = 0 \tag{3-8}$$

Assume that particles size can be determined by radius r (as that said in chapter 2, many kinds radius can be found). If we only focus on the size of the particle, the continuity equation is

$$\frac{\partial n}{\partial t} + \frac{\partial}{\partial r}(v_r n) = 0 \tag{3-9}$$

This is also a generalized form of advection equation.

3-2 Model for Pore Shrinkage

The continuity equation for the population balance on pores is:

$$\frac{\partial n_p(r_p, t)}{\partial t} + \frac{\partial}{\partial r_p}(v_{r_p} n_p(r_p, t)) = 0 \tag{3-10}$$

where r_p (unit: μm) is the pore radius and $n_p(r_p, t)$ (unit: $\mu m^{-3}\mu m^{-1}$) is the number density function of pores. $n_p(r_p, t)dr_p$ is the number of pores whose radius is between r_p and $r_p + dr_p$ at sintering time t.

From Pradip's work [36], the model for pore shrinkage velocity is as follows:

$$v_{r_p} = \frac{dr_p}{dt} = -\frac{k_p}{r_p^m} \tag{3-11}$$

where k_p ($\mu m^{m+1}/h$) is a rate constant and m is a floating model parameter influenced by the material transport mechanism. The minus sign before the formula means shrinkage.

The initial pore size distribution is given by

$$n_p(r_p(0), 0) = n_0(r_0) \tag{3-12}$$

Here $r_0 = r_p(0)$, which means the pore size at the initial time. Combination of equation 3-19 and 3-20 forms the model of pore shrinkage.

Using the solution of this model, we can calculate the total pore volume (which can be used to calculate relative density) and cumulative pore volume distribution (which can be used for comparison).

At sintering time t, the total pore volume $V_p(t)$ (unit: 1) is

$$V_p(t) = C \int_0^\infty n_p(r_p, t) r_p^3 dr_p \tag{3-13}$$

where C is a dimensionless constant for given pore geometry. For example, if we assume that all the pores are spheres, C is $\frac{4\pi}{3}$.

The cumulative pore volume distribution $F_v(r_p, t)$ (unit:1) is defined as the normalized volumes of pores larger than size r_p, i.e.

$$F_v(r_p, t) = \frac{\int_{r_p}^{\infty} n_p(r'_p, t) r'^3_p dr'_p}{\int_0^{\infty} n_0(r_p) r_p^3 dr_p} \tag{3-14}$$

3-2-1 Model Parameter m

m is a floating model parameter influenced by the matter transport mechanism. Although we have introduced the common matter transport mechanisms in Chapter 2, it's hard for us to know which kinds of matter transport mechanism occur in a fixed time point, so the parameter m we used here represents a combination result of all the matter transport mechanisms. It can not only be an integer number, but also non-integer.

Figure 3-1 shows us the pore shrinkage velocity for pores with different sizes. For the small pores, the bigger m is, the faster the pores shrink. For big pores, the shrinkage velocities with different m are very close.

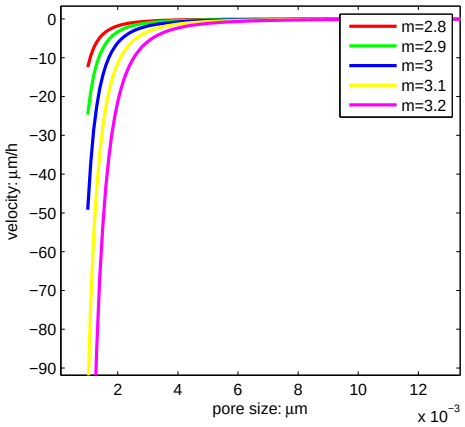

Figure 3-1: Velocity of Pore Shrinkage

Since m is a combination result, it's hard for us to get m directly. It often comes from trial and error of the model calibration.

3-2-2 Rate Constant k_p

The rate constant k_p is only actually constant if all changing during the chemical reaction is the concentration of the reactants. If the temperature or the catalyst is changing, for example, the rate constant will change. Generally, it's decided by Arrhenius equation (See Appendix E).

$$k_p(T) = k_{p0} e^{-\frac{Q_p}{RT}} \tag{3-15}$$

Where Q_p (unit: J/mol) is the activation energy for pore shrinkage (densification). R (unit: $J \cdot K^{-1} mol^{-1}$) is the gas constant. T (unit: K) is the absolute temperature. The units of the pre-exponential factor k_{p0} is identical to the rate constant k_p and will vary depending on the order of the reaction. If the reaction is first order it has the units h^{-1} or s^{-1}.

Q_p can be calculated from the data of Dilato test. k_{p0}, similar to the parameter m, can be got from trial and error. For details on how to get these two parameters, we will discuss later in this chapter.

Figure 3-2 shows the relationship between rate constant k_p and absolute temperature T.

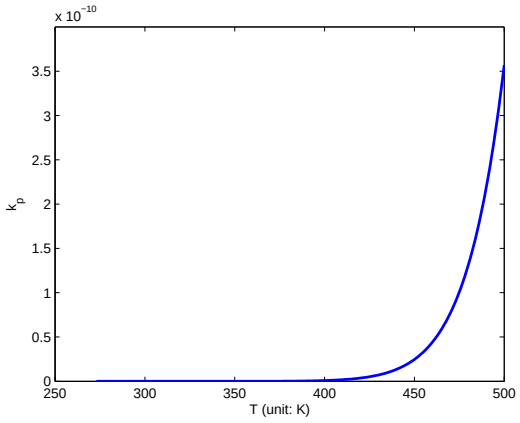

Figure 3-2: Arrhenius Plot 1

The Arrhenius eqaution can be also written as

$$lnk_p = lnk_{p0} - \frac{Q_p}{RT} \tag{3-16}$$

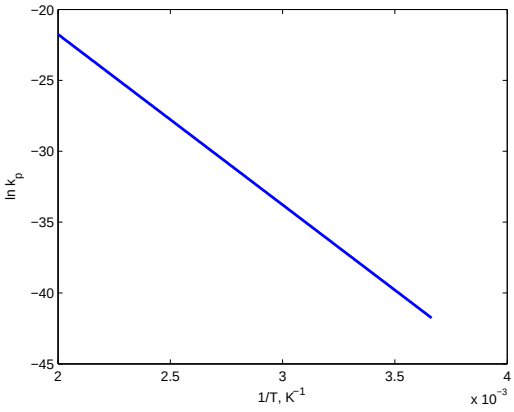

Figure 3-3: Arrhenius Plot 2

The graph between lnk_p and $1/T$ is a straight line with an intercept of $ln(k_{p0})$ and the slop of the graph is equal to $-Q_p/R$. This kind of graph is always used to estimate activation energy.

3-2-3 Initial Distribution

The pore size distribution for a given moment can be interpreted as a histogram of the pore size, which can be got from image analysis.

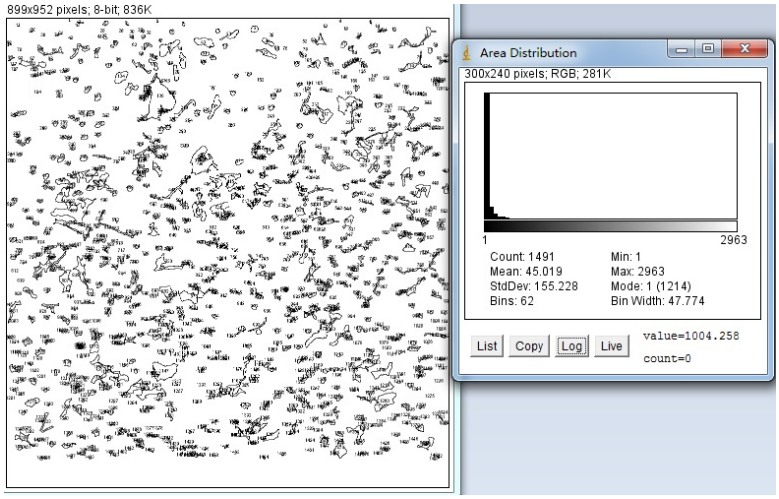

Figure 3-4: Image Analysis

As discussed in Chapter 2, we assume that the initial pore size distribution of alumina is log-normal distribution (see Appendix B):

$$n_0(r) = \frac{1}{r^4\sqrt{2\pi}\ln\sigma} e^{-\frac{1}{2}(\frac{\ln r - \ln r_m}{\ln\sigma})^2} \tag{3-17}$$

where r_m is the number median size and σ is the geometric standard deviation.

3-3 Relative Density

Information from the pore shrinkage model is enough for us to predict the relative density (i.e. there is no need for grain growth model). From Pradip's work [37], the relative density (unit: 1) can be calculated from

$$\rho_r(t) = \frac{1}{1 + \frac{V_p(t)}{V_p(0)}[\frac{1}{\rho_r(0)} - 1]} \tag{3-18}$$

This equation comes from the definition of relative density,

$RelativeDensity = \frac{BulkDensity}{TrueDensity} = \frac{Mass/TotalVolume}{Mass/SolidVolume} = \frac{SolidVolume}{TotalVolume}$

i.e. $\frac{1}{\rho_r} = \frac{V_{solid}+V_p}{V_{solid}} = 1 + \frac{V_p}{V_{solid}}$

$\frac{1}{\rho_r} - 1 = \frac{V_p}{V_{solid}}$

So $\frac{1/\rho_r(t)-1}{1/\rho_r(0)-1} = \frac{V_p(t)V_{solid}(0)}{V_p(0)V_{solid}(t)}$, since $V_{solid}(t) = V_{solid}(0)$, it's easy to transform it into 3-18.

With 3-18, using the results we get in example alumina A16 (see subsection 3-7-1) and the initial relative density 0.62 [37] which is commonly determined from the mass and dimensions, we can get the relative density changing with time.

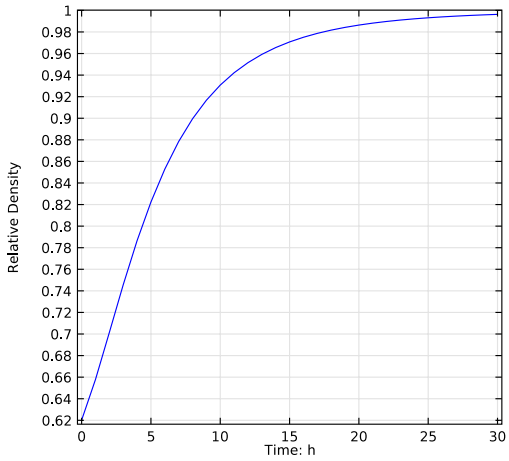

Figure 3-5: Relative Density

3-4 Analytical Solution

Now we go back to the model,

$$\frac{\partial n_p(r_p,t)}{\partial t} + \frac{\partial}{\partial r_p}(v_{r_p} n_p(r_p,t)) = 0 \tag{3-19}$$

$$v_{r_p} = \frac{dr_p}{dt} = -\frac{k_p}{r_p^m} \tag{3-20}$$

$$n_p(r_p(0),0) = n_0(r_0) \tag{3-21}$$

Solving equation 3-20, we can get that

$$v_{r_p} = \frac{dr_p}{dt} = -\frac{k_p}{r_p^m} \tag{3-22}$$

$$\Rightarrow r_p^m dr = -k_p dt \tag{3-23}$$

$$\Rightarrow \frac{r_p^{m+1}}{m+1}|_{r_p(0)}^{r_p(t)} = -\int_0^t k_p dt \tag{3-24}$$

Note that in last section we introduce k_p as a variable related with temperature T. But T is changing over time, so k_p can be also viewed as a function of time t. Then

$$r_p(0) = [r_p^{m+1}(t) + (m+1)\int_0^t k_p dt]^{\frac{1}{m+1}} \tag{3-25}$$

Also from equation 3-20, we can get that

$$\Rightarrow \frac{dr_p(0)}{dr_p(t)} = (\frac{r_p(t)}{r_p(0)})^m \tag{3-26}$$

Besides, equation 3-19 can be solved by a transformation technique [36]. We assume that the pores with same size will have same shrinkage rate. The number of pores whose radius are same in the beginning will keep the same at sintering time t. Then the equation 3-27 holds for all time t. This is stronger than 3-19, which means that solution derived from this equation can be also used as the solution of 3-19.

$$n_p(r_p(t), t)dr_p(t) = n(r_p(0), 0)dr_p(0) \tag{3-27}$$

Substitute equation 3-26, 3-27 into 3-21, we can get

$$n_p(r_p(t), t) = \frac{n_0([r_p^{m+1} + (m+1)\int_0^t k_p(t')dt']^{1/(m+1)})}{(1 + (m+1)r_p^{-(m+1)}\int_0^t k_p(t')dt')^{m/(m+1)}} \tag{3-28}$$

If k_p is a constant, all the $\int_0^t k_p dt'$ shown in the above equations can be replaced by $k_p t$, the analytical solution is

$$n_p(r_p(t), t) = \frac{n_0([r_p^{m+1} + (m+1)k_p t]^{1/(m+1)})}{(1 + (m+1)k_p t r_p^{-(m+1)})^{m/(m+1)}} \tag{3-29}$$

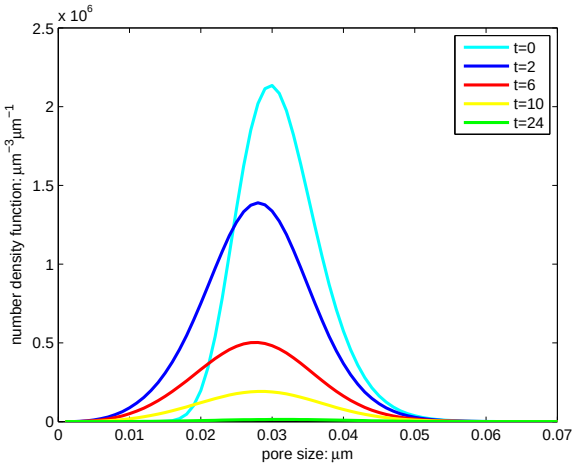

Figure 3-6: Plot of Analytical Solution

If we choose the initial distribution as:

$$n_0(r) = \frac{1}{r^4\sqrt{2\pi}\ln\sigma} e^{-\frac{1}{2}(\frac{\ln r - \ln r_m}{\ln \sigma})^2} \tag{3-30}$$

where geometric mean radius $r_m = 0.034\mu m$ and geometric standard deviation $\sigma = 1.2$. And to make problem simple, we use a constant k_p here. The parameter m and k_p in the model is $m = 3, k_p = 4.92 * 10^{-8}\mu m^4/h$. The plot of analytical solution is shown in Figure 3-6.

We can use the analytical solution to check the subsequent numerical computations.

3-5 Numerical Solution with Two ODEs

Substitute 3-20 into 3-19,

$$\frac{\partial n_p(r_p,t)}{\partial t} + \frac{\partial}{\partial r_p}(-\frac{k_p}{r_p^m} n_p(r_p,t)) = 0 \tag{3-31}$$

$$\Rightarrow \frac{\partial n_p(r_p,t)}{\partial t} + n_p(r_p,t)\frac{k_p m}{r_p^{m+1}} - \frac{k_p}{r_p^m}\frac{\partial n_p(r_p,t)}{\partial r_p} = 0 \tag{3-32}$$

$$\Rightarrow \frac{\partial n_p(r_p,t)}{\partial t} + n_p(r_p,t)\frac{k_p m}{r_p^{m+1}} + \frac{dr_p}{dt}\frac{\partial n_p(r_p,t)}{\partial r_p} = 0 \tag{3-33}$$

$$\Rightarrow \frac{\partial n_p(r_p,t)}{\partial t} + \frac{dr_p}{dt}\frac{\partial n_p(r_p,t)}{\partial r_p} = -n_p(r_p,t)\frac{k_p m}{r_p^{m+1}} \tag{3-34}$$

Then

$$\frac{dn_p}{dt} = \frac{\partial n_p}{\partial t} + \frac{\partial n_p}{\partial r_p}\frac{\partial r_p}{\partial t} = -n_p(r_p,t)\frac{k_p m}{r_p^{m+1}} \tag{3-35}$$

Now we change the problem into 2 Ordinary Differential Equation (ODE) model

$$\frac{dr_p}{dt} = -\frac{k_p}{r_p^m} \tag{3-36}$$

$$\frac{dn_p}{dt} = -n_p(r_p,t)\frac{k_p m}{r_p^{m+1}} \tag{3-37}$$

With the same initial distribution and parameters as that in last section (same as Figure 3-6), solving 3-36 and 3-37 with finite difference method (forward Euler).

$$\frac{r_p(t(n+1)) - r_p(t(n))}{\Delta t} = -\frac{k_p(t(n))}{r_p^m(t(n))} \tag{3-38}$$

$$\frac{n_p(r_p(t(n+1)),t(n+1)) - n_p(r_p(t(n)),t(n))}{\Delta t} = -n_p(r_p(t(n)),t(n))\frac{k_p(t(n))m}{r_p^{m+1}(t(n))} \tag{3-39}$$

If we use equidistant time interval, some times negative value of r_p my occur, which doesn't match the situation in the real world. So the time interval we choose here is not equidistant. We assume that the smallest pore will vanish first, then the first time interval equals to the time for the smallest pore to vanish. Then the first value of new generated r_p and n_p must be zero. We start to use forward euler method from the second value. The next time interval is got in the same way using the updated values of r_p. Again and again, we can get all the time intervals and values corresponding to the time points. Since we use different time interval, to get the number density values at other time points, we use interpolation.

The plot of solutions is as follows:

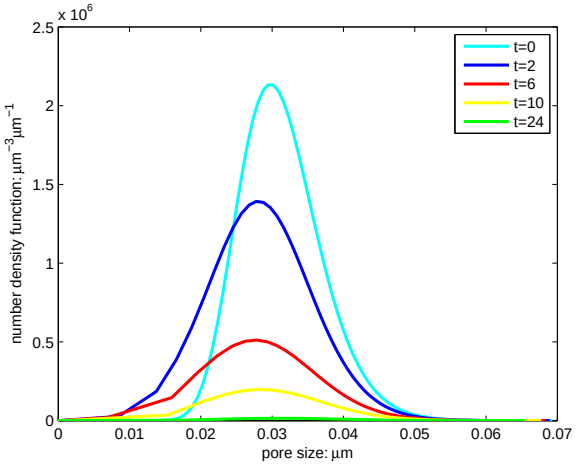

Figure 3-7: Plot of Numerical Solution (two ODEs model)

We can see that on the left of the figure, the curves are not so smooth. This is because there are too many zeros during the interpolation. If we want to get more accurate solutions, we can discard the zero values after fixed number of iterations and reconstruct the remaining size distribution. Since the purpose of introduing ODE models is for comparison, the above result is enough.

3-6 Numerical Solution with Finite Element Method(FEM)

3-6-1 Conventional Galerkin Method

The underlying finite element discretization method in COMSOL Multiphysics is the Galerkin method. [38] For the following problem,

$$\begin{cases} \frac{\partial n_p(r_p,t)}{\partial t} + \frac{\partial}{\partial r_p}(v_{r_p} n_p(r_p,t)) = 0 \quad on \quad [0,L] \\ n_p(r_p,0) = n_0(r_p) \quad on \quad [0,L] \\ n_p(r_p=0,t) = 0 \\ n_p(r_p=L,t) = 0 \end{cases} \tag{3-40}$$

Multiplying the first equation by test function w ($w(0) = 0 = w(L)$) and integrating on the whole domain, we have

$$\int_0^L \frac{\partial n_p(r_p,t)}{\partial t} w dr_p + \int_0^\infty \frac{\partial}{\partial r_p}(v_{r_p} n_p(r_p,t)) w dr_p = 0 \tag{3-41}$$

$$\int_0^L \frac{\partial n_p(r_p,t)}{\partial t} w dr_p + w v_{r_p} n_p(r_p,t)|_{r_p=0}^L - \int_0^L (v_{r_p} n_p(r_p,t)) \frac{\partial w}{\partial r_p} dr_p = 0 \tag{3-42}$$

$$\int_0^L \frac{\partial n_p(r_p,t)}{\partial t} w dr_p - \int_0^L (v_{r_p} n_p(r_p,t)) \frac{\partial w}{\partial r_p} dr_p = 0 \tag{3-43}$$

This is the weak form of the original equation. Further we take basis functions (piecewise linear), $\phi_i(0) = \phi_i(L) = 0$ for $i = 1, 2, \ldots, s-1$

$$n_p(r_p, t) = \Sigma_{j=1}^{s-1}[n_{p_j}(t)\phi_j(r_p)] + n_{p_0}(t)\phi_0(r_p) + n_{p_L}(t)\phi_s(r_p) \tag{3-44}$$

According to the boundary condition,

$$n_p(r_p, t) = \Sigma_{j=1}^{s-1}[n_{p_j}(t)\phi_j(r_p)] \tag{3-45}$$

then

$$\Sigma_{j=1}^{s-1}[n'_{p_j}(t)\int_0^L \phi_j(r_p)\phi_i(r_p)dr_p] = \Sigma_{j=1}^{s-1}[n_{p_j}(t)\int_0^L v_{r_p}\phi_j(r_p)\phi'_i(r_p)dr_p], \quad i = 1, 2, \ldots, s-1 \tag{3-46}$$

For backward Euler,

$$\Sigma_{j=1}^{s-1}[\frac{n_{p_j}^{n+1} - n_{p_j}^n}{\Delta t}\int_0^L \phi_j(r_p)\phi_i(r_p)dr_p] = \Sigma_{j=1}^{s-1}[n_{p_j}^{n+1}(t)\int_0^L v_{r_p}\phi_j(r_p)\phi'_i(r_p)dr_p] \tag{3-47}$$

$i = 1, 2, \ldots, s-1$. Elementwise, we obtain

$$\frac{n_{p_{i-1}}^{n+1} - n_{p_{i-1}}^n}{\Delta t}\int_{e_i}\phi_i\phi_{i-1}dr_p + \frac{n_{p_i}^{n+1} - n_{p_i}^n}{\Delta t}\int_{e_i\cup e_{i+1}}\phi_i^2 dr_p + \frac{n_{p_{i+1}}^{n+1} - n_{p_{i+1}}^n}{\Delta t}\int_{e_{i+1}}\phi_i\phi_{i+1}dr_p \tag{3-48}$$

$$= n_{p_{i-1}}^{n+1}\int_{e_i} v_{r_p}\phi_{i-1}\phi'_i dr_p + n_{p_i}^{n+1}\int_{e_i\cup e_{i+1}} v_{r_p}\phi_i\phi'_i dr_p + n_{p_{i+1}}^{n+1}\int_{e_{i+1}} v_{r_p}\phi_{i+1}\phi'_i dr_p \tag{3-49}$$

Let $M_{ij} = \int_0^L \phi_i\phi_j dr_p$ and $S_{ij} = \int_0^L v_{r_p}\phi_i\phi'_j dr_p$, Matrix M is called mass-matrix [39] and S is called Stiffness Matrix [39]. The above finite element discretization problem can be written in matrix form as

$$M\frac{dc}{dt} = Sc, \quad c = [n_{p_1}, n_{p_2}, \ldots, n_{p_n}]^T \tag{3-50}$$

Using backword-Euler method, it can be rewritten as

$$Mc^{n+1} = Mc^n + \Delta t Sc^{n+1} \tag{3-51}$$

where $M = \begin{pmatrix} \int_0^L \phi_1^2 dr_p & \int_0^L \phi_1\phi_2 dr_p & 0 & 0 & \cdots & 0 & 0 \\ \int_0^L \phi_2\phi_1 dr_p & \int_0^L \phi_2^2 dr_p & \int_0^L \phi_2\phi_3 dr_p & 0 & \cdots & 0 & 0 \\ 0 & \int_0^L \phi_3\phi_2 dr_p & \int_0^L \phi_3^2 dr_p & \int_0^L \phi_3\phi_4 dr_p & \cdots & 0 & 0 \\ \vdots & \vdots & \ddots & \ddots & \ddots & \vdots & \vdots \\ 0 & 0 & 0 & 0 & \cdots & \int_0^L \phi_{s-2}^2 & \int_0^L \phi_{s-2}\phi_{s-1}dr_p \\ 0 & 0 & 0 & 0 & \cdots & \int_0^L \phi_{s-1}\phi_{s-2}dr_p & \int_0^L \phi_{s-1}^2 dr_p \end{pmatrix}$

$$\text{and } S = \begin{pmatrix} \int_0^L v_{r_p}\phi_1\phi_1' dr_p & \int_0^L v_{r_p}\phi_2\phi_1' dr_p & 0 & \cdots & 0 & 0 \\ \int_0^L v_{r_p}\phi_2\phi_1' dr_p & \int_0^L v_{r_p}\phi_2\phi_2' dr_p & \int_0^L v_{r_p}\phi_3\phi_2' dr_p & \cdots & 0 & 0 \\ 0 & \int_0^L v_{r_p}\phi_2\phi_3' dr_p & \int_0^L v_{r_p}\phi_3\phi_3' dr_p & \cdots & 0 & 0 \\ \vdots & \ddots & \ddots & \ddots & \vdots & \vdots \\ 0 & 0 & 0 & \cdots & \int_0^L v_{r_p}\phi_{s-2}\phi_{s-2}' dr_p & \int_0^L v_{r_p}\phi_{s-1}\phi_{s-2}' dr_p \\ 0 & 0 & 0 & \cdots & \int_0^L v_{r_p}\phi_{s-2}\phi_{s-1}' dr_p & \int_0^L v_{r_p}\phi_{s-1}\phi_{s-1}' dr_p \end{pmatrix}$$

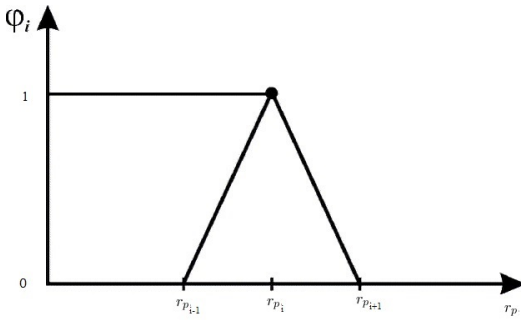

Figure 3-8: Piecewise Linear Function $\phi_i(r_p)$

3-6-2 Streamline Diffusion

A problem shown in Figure 3-9 is that even if we use extremely fine mesh, there still exists some wiggle after sufficient time. We change the tolerance (AT is absolute tolerance, RT is relative tolerance) and time step into smaller pieces, it doesn't work.

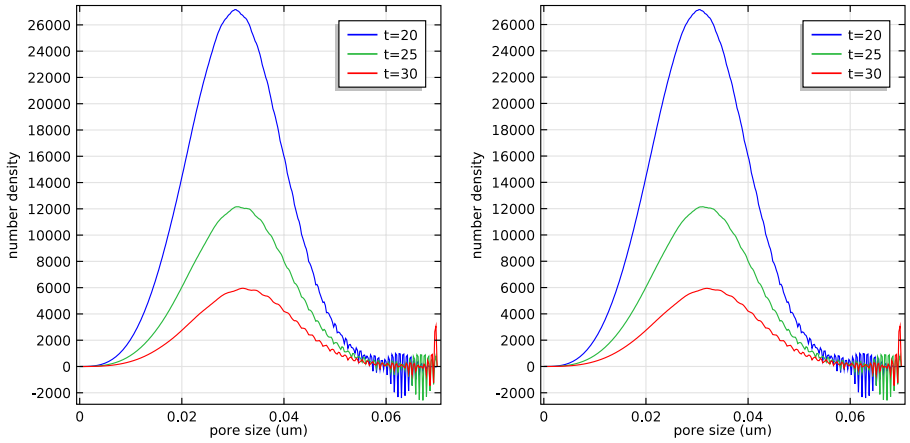

(a) timestep=0.1, $AT = 10^{-4}, RT = 10^{-3}$

(b) timestep=0.001, $AT = 10^{-6}, RT = 10^{-5}$

Figure 3-9: Number Density Function with Different Time Step and Tolerance Value

This is because the Partial Differential Equation (PDE) in our problem has no diffusion part.

Such equations are unstable if discretized using the Galerkin finite element method. For equation

$$\frac{\partial u}{\partial t} + \beta \nabla u = \nabla(c \nabla u) + su + F \tag{3-52}$$

Element Péclet number (Pe) [38] is $Pe = \frac{\|\beta\| h}{2c}$. Element Damköhler number [38] is $Da = \frac{|s|h}{\|\beta\|}$. The solution is unstable if $2DaPe = \frac{|s|h^2}{c} > 1$. In our case c is 0, so $2DaPe$ is always larger than 1. The conventional Galerkin method is unstable [38]. So we need to use stabilized finite element methods to obtain physical solutions.

For the advection dominated problem, the conventional Galerkin method cannot produce optimal approximation [14]. To solve this problem, we introduce streamline diffusion method. The streamline diffusion method is a consistent stabilization method in COMSOL [38], including the Streamline-Upwind/Petrov-Galerkin (SUPG) method and Galerkin Least-Squares (GLS) method. The main idea of these two methods is to add products of suitable perturbation terms and the residuals, thereby maintaining consistency [40]. In a conventional Galerkin weighted residual method, the weighting functions are considered to be continuous across inter element boundaries. The streamline upwind/Petrov-Galerkin formulation, however, requires discontinuous weighting functions of the form.

The SUPG method, introduced from Brooks and Hughes in [14], is the first successful stabilization technique to prevent oscillations in advection-dominated problems in finite element method. In the SUPG method, the weighting function for a typical node is modified to weight element upwind of the node more heavily than the downwind element, as shown in the following figure:

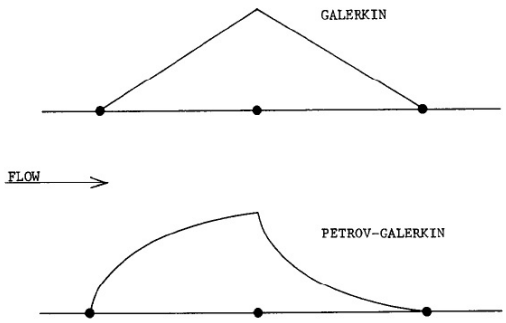

Figure 3-10: Piecewise Linear Function (Conventional Galerkin and SUPG)[14]

Galerkin Least-Squares (GLS) is a more advanced version of SUPG. It's also a consistent method and has the same order of accuracy as SUPG [14].

COMSOL has supplied lots of existing models for different situations, so it's not necessary for us to rewrite the weak form by ourselves. To use streamline diffusion method, we start from $(ModelWizard > 1D > Chemical\ \ Species\ \ Transport > Thansport\ \ of\ \ Diluted\ \ Spieces(chds)$. Then we choose 'convection' under transport mechanism, 'streamline diffusion' under consistent stabilization and 'Conservative form' under Advanced setting in COMSOL 4.3a. The results are as follows:

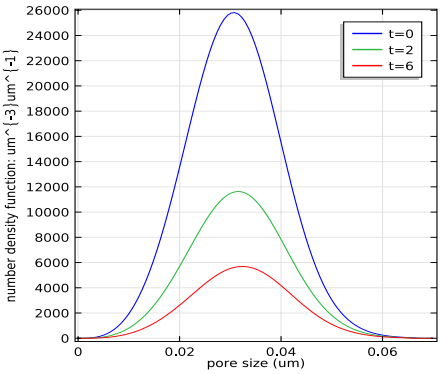

Figure 3-11: Solution with GLS

Compared with results using conventional Galerkin method (shown in Figure 3-9), we can see that the oscillation problem has been solved.

3-7 Numerical Examples

The parameter values and initial distributions used in the following two examples are from Pradip's work [37].

3-7-1 Example 1: Alumina 16

Parameters in the model are $m = 3, k_p = 4.92{*}10^{-8}\mu m^4/h, r_m = 0.034\mu m, \sigma = 1.2$. Comparison results from Figure 3-12 and Figure 3-13 have the same shape and very close values. This is a very strong indication that our solutions in COMSOL is a 'good' simulation.

The graphs of number density function of pores show a decrease of average pore size in time. The graphs of the cumulative distribution function show that small pores decrease faster than big ones, which is the same as what we get from velocity analysis earlier in this chapter.

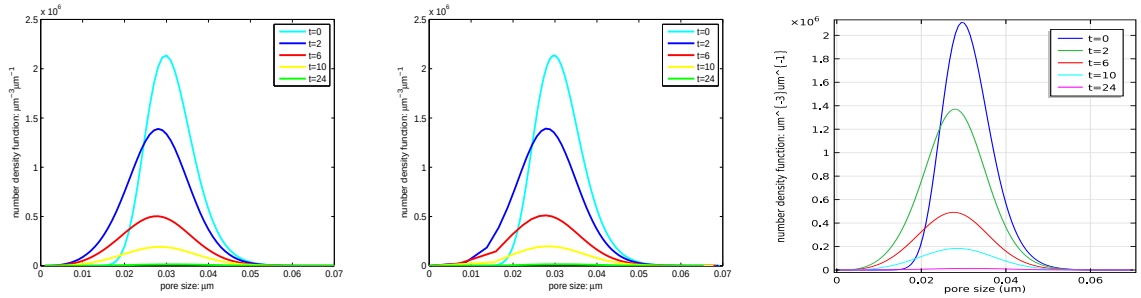

(a) analytical result (b) 2-ODE model (c) FEM result

Figure 3-12: Number Density Function of Pores - Alumina A16

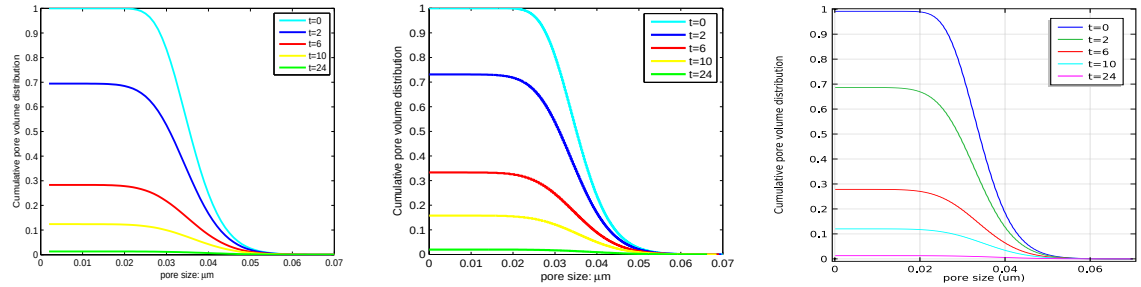

(a) analytical result (b) 2-ODE model (c) FEM result

Figure 3-13: Cumulative Pore Volume Distribution - Alumina A16

3-7-2 Example 2: Zirconia SYP 5.2

Change the parameters into $m = 1, k_p = 0.43\mu m^2/h, r_m = 4\mu m, \sigma = 1.4$. Comparing with the analytical results and results generated from matlab, what we get from FEM produces a better approximation than 2-ODEs. It's not clear in the number density graphs, but in the cumulative pore volume distribution graphs, we can see that the results of analytical solution and FEM solution are the same, while the results from 2-ODE model have significant error.

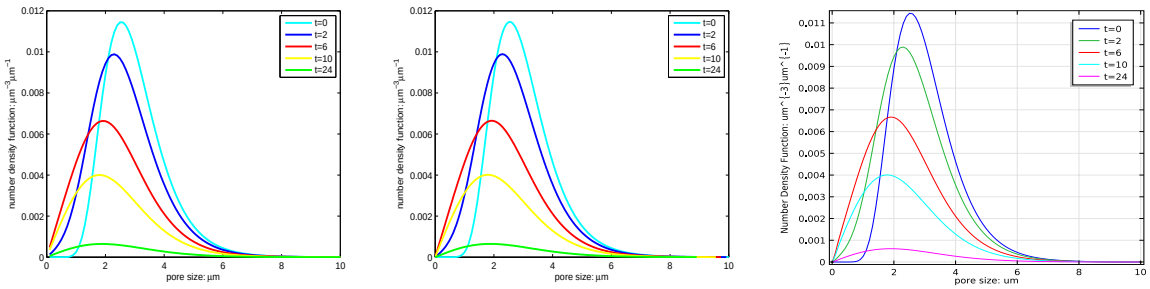

(a) analytical result (b) 2-ODE model (c) FEM result

Figure 3-14: Number Density Function of Pores - Zirconia SYP 5.2

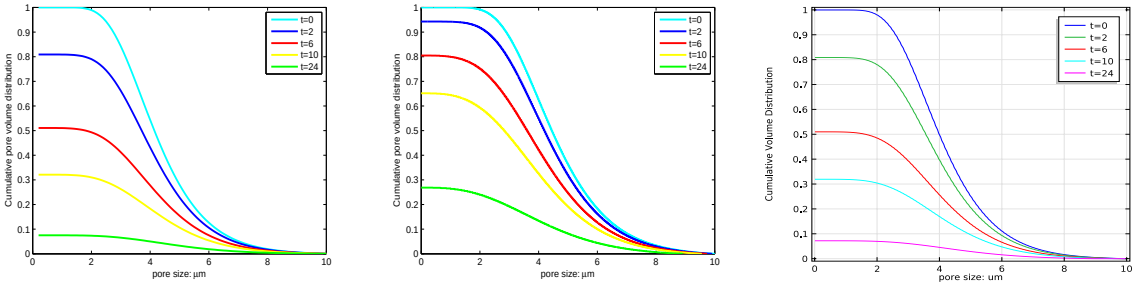

(a) analytical (b) 2-ODE model (c) FEM result

Figure 3-15: Cumulative Pore Volume Distribution - Zirconia SYP 5.2

Similar to the previous example. The graphs of number density function of pores show a decrease of pore size in time. The graphs of the cumulative distribution function show that small pores decrease faster than big ones, which is the same as what we get from velocity analysis earlier in this chapter.

3-8 Sensitive Analysis

Here we use Alumina A16 as an example:

$$r_m = 0.034\mu m, \sigma = 1.2, m = 3, k_p = 4.92 * 10^{-8}\mu m^4/h.$$

The velocity and number density is shown in Figure 3-16. From these two sub-figures we can see that the smaller the pore size is, the faster it shrinks.

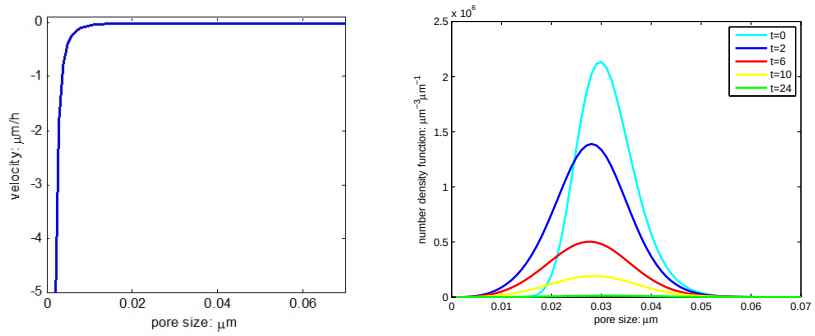

(a) velocity (b) number density

Figure 3-16: Velocity and Number Density Function

Now we change the parameters m and k_p and see how the solution performs.

3-8-1 m Change

If we change m from 3 to 4 (or 3 to 2, see Figure 3-17), it's a little bit hard for us to compare the velocity in one figure.

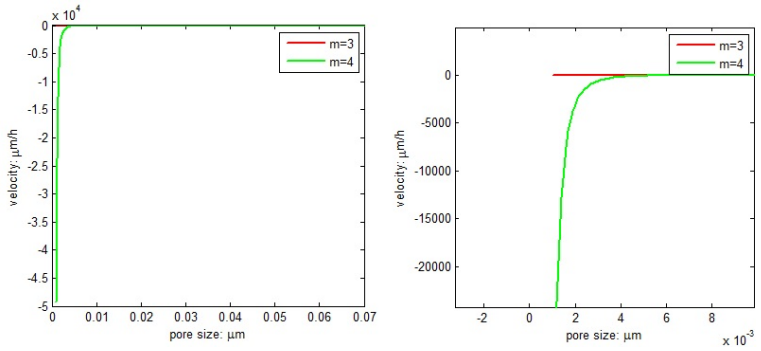

Figure 3-17: Velocity Changing with m, m is 3,4

So we choose a smaller range from 2.8 to 3.2 (see Figure 3-18).

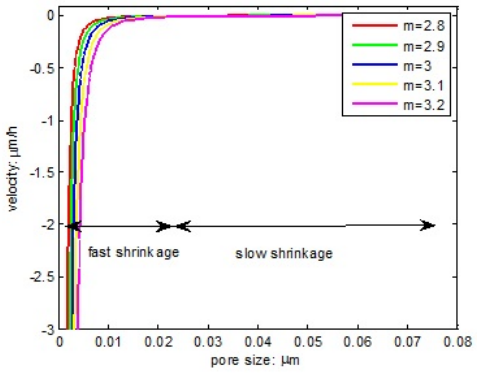

Figure 3-18: Velocity Changing with m, m is 2.8 3.2

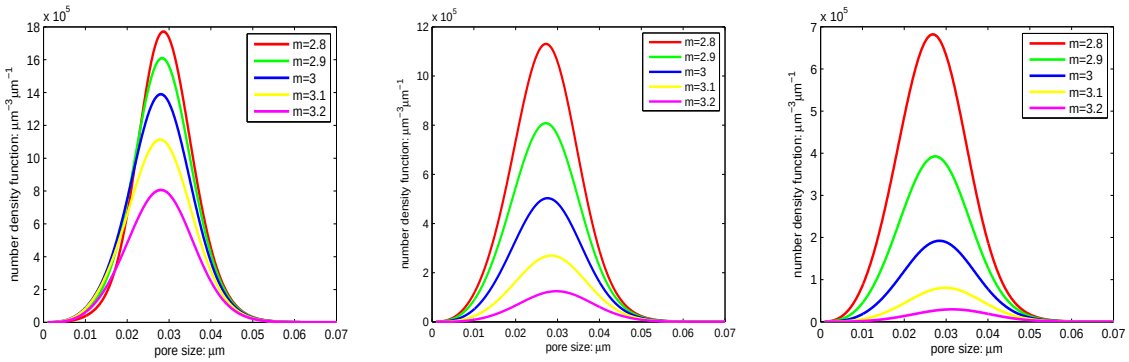

(a) after 2h (b) after 6h (c) after 10h

Figure 3-19: Number Density Changing with m

From Figure 3-18 we can see that for smaller pores, the larger m is, the faster the shrinkage rate is. while for big pores, the changing of pore shrinkage velocity is not so clear. This can be also illustrated in the figure of number density function (see Figure 3-19).

3-8-2 k_p Change

Similar to the reason we choose the range for m change, we now change the value for parameter k_p from $1 * 10^{-8}$ to $11 * 10^{-8}$.

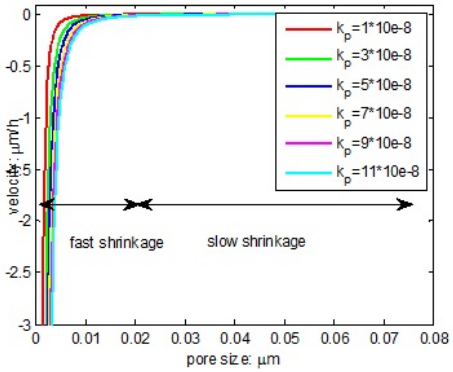

Figure 3-20: Velocity Changing with k_p

From Figure 3-20 we can see that for smaller pores, the larger k_p is, the faster the shrinkage rate is. While for big pores, the changing of pore shrinkage velocity is not so clear. This can be also illustrated in the figure of number density function (see Figure 3-21).

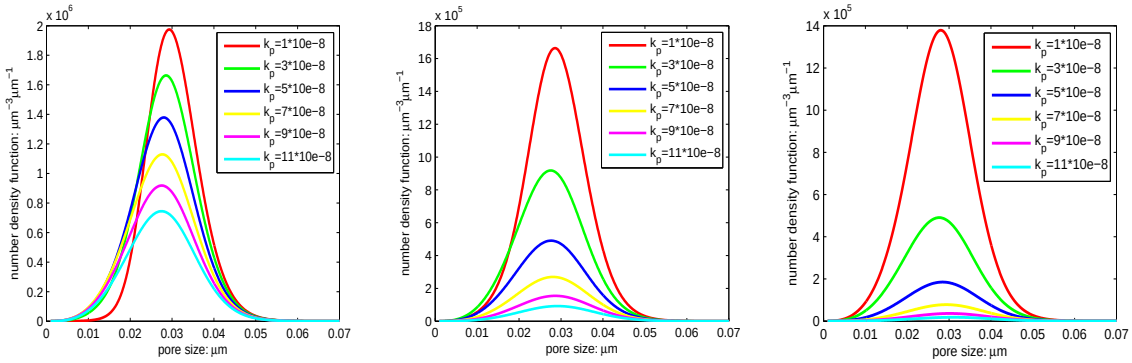

(a) after 2h (b) after 6h (c) after 10h

Figure 3-21: Number Density Changing with k_p

3-9 Application

Until now we've got enough information on the model of pore shrinkage. First we introduced the basic concept of the pore shrinkage model and corresponding parameters. Secondly, we introduced three different solutions to this model (analytical solution, numerical solution with two ODEs and numerical solution with FEM). Then using data from some existing literature, we validate the model with two examples and do sensitive analysis. In this section we focus on how to use the real data to get all the parameters and variables needed in the model step by step and show the comparison result of the model and the real data.

3-9-1 Initial Pore Size Distribution of Alumina

As discussed in Chapter 2, we assume that the initial pore size distribution of alumina is log-normal distribution:

$$n_0(r) = \frac{1}{r^4\sqrt{2\pi}\ln\sigma} e^{-\frac{1}{2}(\frac{\ln r - \ln r_m}{\ln\sigma})^2} \tag{3-53}$$

where r_m is the number median size and σ is the geometric standard deviation.

Earlier in this chapter, we said that the distribution can be got from image analysis. Now we use an example to show how to do it.

There are several kinds of methods and corresponding softwares used to do image analysis. In this project, we use the software Image J [2].

For the Figure 3-22, we use the software Image J to analyze the pore size and get the following result:

The mean value of area diameter is 45.019px ($\approx 64.313\mu m$), and the standard deviation is 155.228px ($\approx 221.754\mu m$). However, this result may be far away from the accurate value, because some too large values have to be gave up. Besides, lots of the area values are 1px, which means that we may need the SEM figure with larger amplification factor. Giving up the values larger than 1000px, we calculate the geometric mean and geometric standard deviation and get the results $r_m = 3.747\mu m, \sigma = 5.925$.

So the initial pore size distribution is

$$n_0(r) = \frac{1}{r^4\sqrt{2\pi}\ln\sigma} e^{-\frac{1}{2}(\frac{\ln r - \ln r_m}{\ln\sigma})^2} \tag{3-54}$$

[2]Image J is a public domain Java image processing program inspired by NIH Image for the Macintosh [41]. http://rsbweb.nih.gov/ij/index.html

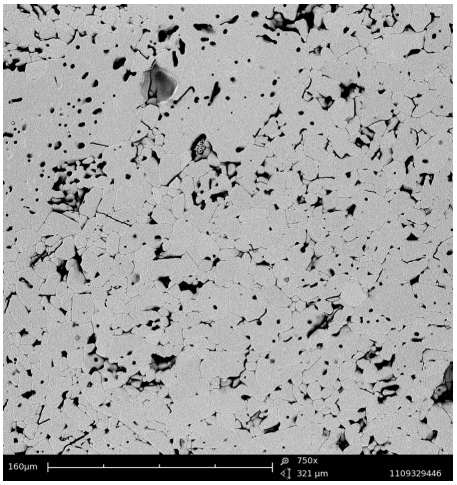

Figure 3-22: SEM Image

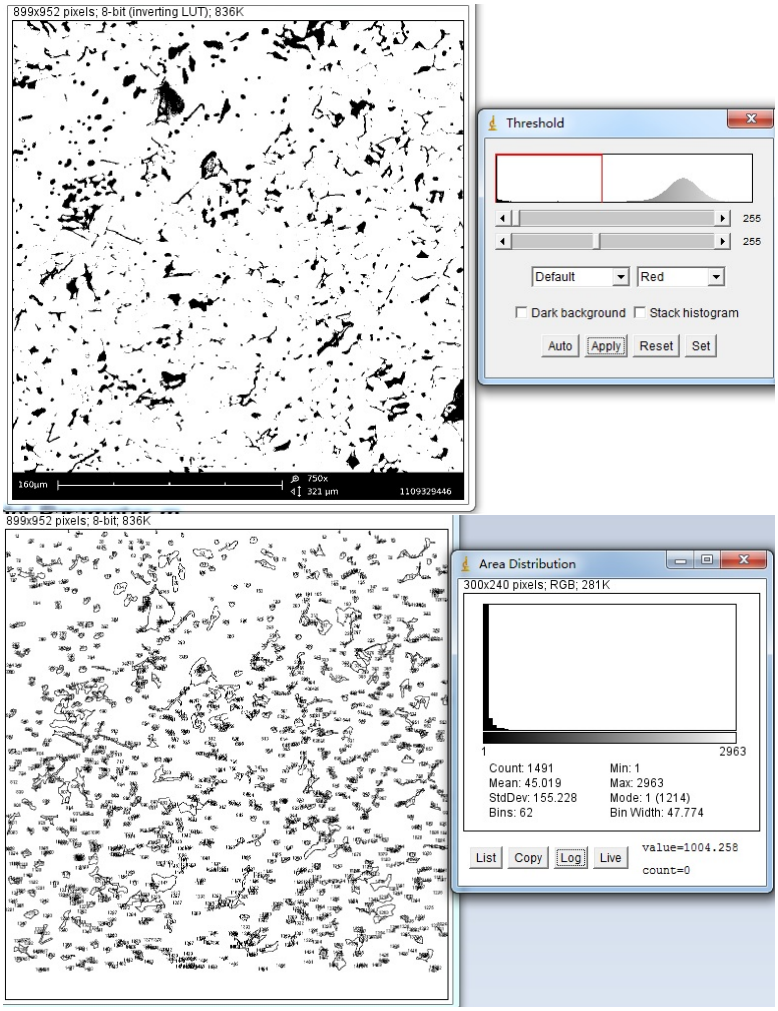

Figure 3-23: Image Analysis

with $r_m = 3.747\mu m$ and $\sigma = 5.925$.

3-9-2 Initial Relative Density of Alumina

As to the initial relative density of alumina, we use the value from some other literatures [42] [43]. The initial relative density of α-alumina is 0.5 or 0.62.

3-9-3 Rate Constant k_p

We've already known that k_p is decided by Arrhenius equation (See Appendix E).

$$k_p(T) = k_{p0} e^{-\frac{Q_p}{RT}} \tag{3-55}$$

The gas constant R is $8.314 J \cdot mol^{-1} \cdot K^{-1}$. we still need to know the activation energy Q_p and the pre-exponential parameter k_{p0}.

Theory of Estimating Activation Energy

Simón Yobanny Reyes Lópeza, Juan Serrato Rodríguezb and Satoshi Sugita Sueyoshic introduced a method to calculate densification activation energy in 2011 [44]. Their idea is as follows:

In general, the densification rate can be separated into temperature and density [45] [46].

$$\frac{d\rho}{dt} = k_{p0} \frac{e^{-\frac{Q_p}{RT}}}{T} f(\rho) \tag{3-56}$$

Where $d\rho/dt$ is the instantaneous rate of densification, R is the gas constant, T is the absolute temperature, Q_p is the activation energy for densification, f(ρ) is a function of density and k_{p0} is a material parameter that is insensitive to ρ.

Densification rates may be written as:

$$\frac{d\rho}{dt} = \frac{d\rho}{dT} T' \tag{3-57}$$

Substitute 3-57 into 3-56,

$$\ln(TT' \frac{d\rho}{dT}) = -\frac{Q_p}{RT} + \ln(f(\rho)) + k_{p0} \tag{3-58}$$

A plot of $\ln(TT' \frac{d\rho}{dT})$ v.s. $\frac{1}{T}$ would give a value for Q_p. This can be got from the data of Dilato test.

Example of Estimating Activation Energy

We take an example from the lab for example. The raw material is KA-13 used in Ludwigshafen of Almatis.

If we want to plot $\ln(TT'\frac{d\rho}{dT})$ vs $\frac{1}{T}$, we need temperature cycle and the relative density calculated from experiment data.

Temperature cycle in the lab is as follows:

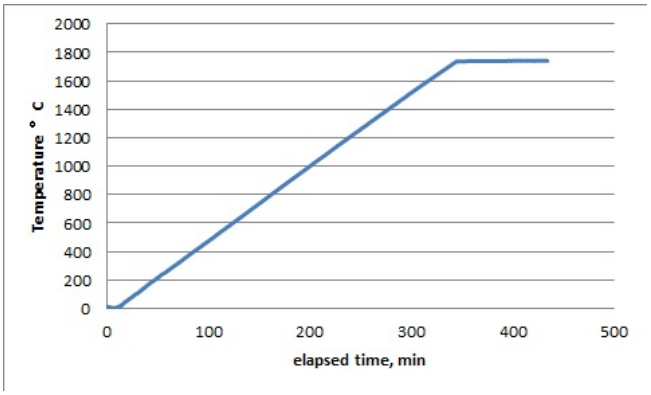

Figure 3-24: Temperature Cycle

As to calculating the relative density changing over temperature (or time) in the experiment, we need to know what we can get directly from the experiment. From Dilato test, we can get relative expansion, which is similar to that shown in Figure 2-11. Now what we need to do is to find out the relationship between the relative expansion and relative density. Here we introduce two new concepts: thermal expansion coefficient and shrinkage rate, then we'll show the relationship among thermal expansion coefficient, shrinkage rate and relative density (densification curve).

The degree of expansion (for certain material) decided by the change in temperature is called the thermal expansion coefficient (α) and generally varies with temperature.

True thermal expansion coefficient

$$\alpha_v = \frac{1}{V_0}(\frac{\partial V}{\partial T})_P \tag{3-59}$$

- V_0 - initial volume
- V - volume
- T - temperature
- p - indicates that the pressure is held constant during the expansion

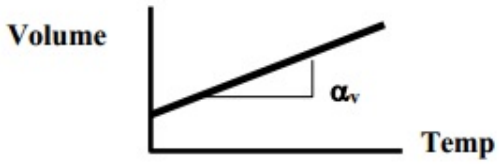

Figure 3-25: Thermal Expansion Coefficient

More common use is the average thermal expansion coefficient, defined by a change in volume over a specified temperature range:

$$\alpha_v = \frac{1}{V_0}\frac{\Delta V}{\Delta T} \tag{3-60}$$

- V_0 - initial volume
- ΔV - change in volume
- ΔT - change in temperature

Since volume change is difficult to measure, linear change is much more simple and a typical thermal expansion coefficient is based on a length-change measurement:

$$\alpha = \frac{1}{L_0}\frac{\Delta L}{\Delta T} \tag{3-61}$$

- α - coefficient of expansion
- L_0 - initial sample length
- ΔL - change in length
- ΔT - change in temperature

We can assume that during sample cooling sintering doesn't take place, then the cooling shrinkage is only dependent on thermal dilatation and we can calculate the thermal expansion coefficient [47].

$$\alpha = \frac{\epsilon_{room} - \epsilon_{Tmax}}{(T_{room} - T_{max}) * 100} \tag{3-62}$$

where

- ϵ_{room} - the shrinkage after cooling (%)
- ϵ_{Tmax} - the shrinkage at the end of dwell (%)
- T_{room} - the temperature after cooling (°C)
- T_{max} - the temperature at the end of dwell (°C)

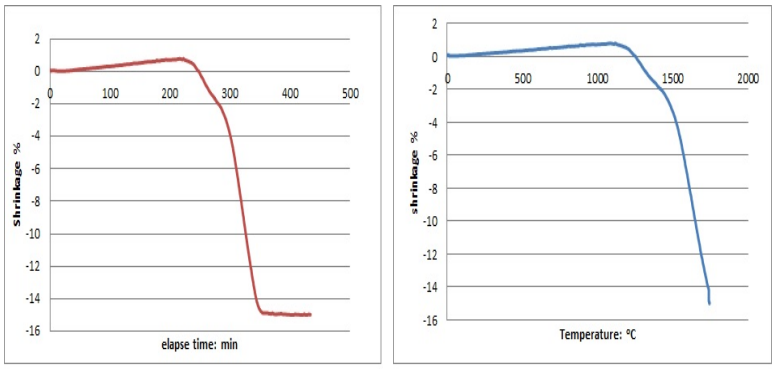

(a) Shrinkage V.S. Time (b) Shrinkage V.S. Temperature

Figure 3-26: Shrinkage

Compared with the result of Dilato test, we can find that equation 3-60 is our best choice. And we come back to the experiment data.

At low temperature only thermal dilatation of the green body happens. When a certain temperature is reached the sintering process begins and the material starts to shrink. As long as the temperature increases the thermal dilatation continues as well. So we can take first (increasing) part of the shrinkage curve to calculate thermal expansion coefficient, because we assume that in this part only thermal dilatation of the green body happens. From Figure 3-27, we can see that the thermal expansion coefficient is $7 * 10^{-6} K^{-1}$.

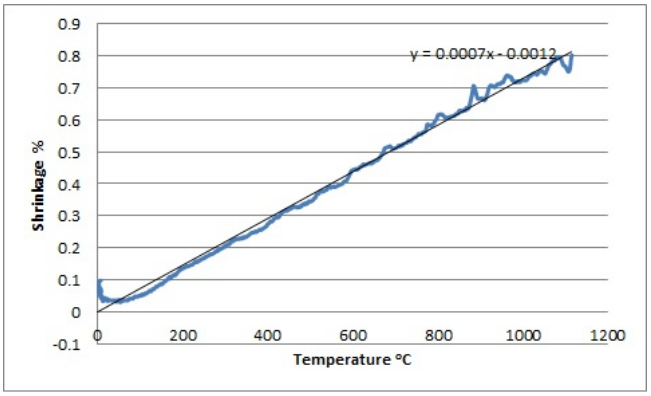

Figure 3-27: Thermal Expansion Coefficient from Experiment

In Cho Yen Ho and Richard Erwin Taylor' book[48], the thermal expansion coefficient of α-alumina at room temperature is in the range about $5 * 10^{-6} K^{-1}$. Comparing this value with our result, we can see that the value we calculated from the experiment data is reasonable.

Since we only want to get the activation energy for pore shrinkage caused by sintering, we need to subtract the shrinkage caused by thermal dilatation and get the sintering shrinkage (also

called technological shrinkage) [47].

$$\epsilon_{tech}(t,T) = \epsilon(t,T) - \alpha * 100 * (T - T_{room}) \tag{3-63}$$

where

- $\epsilon_{tech}(t,T)$ - the shrinkage at time t (temperature T)
- t - time
- T - temperature (°C)
- T_{room} - 25 °C

Using the thermal expansion coefficient calculated before ($\alpha = 7 * 10^{-6}K^{-1}$), the sintering shrinkage result is shown as follows:

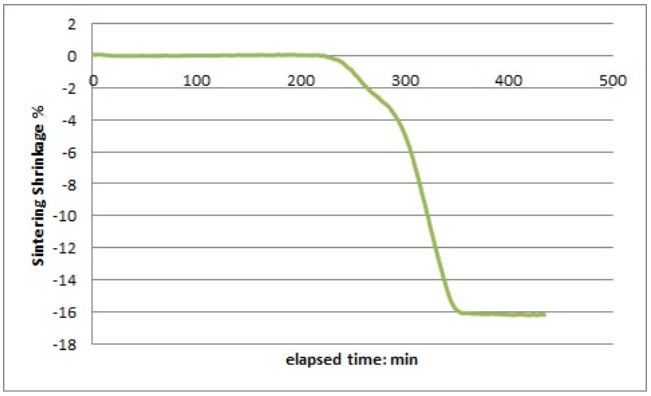

Figure 3-28: Sintering Shrinkage

Next step is to calculate relative density with the sintering shrinkage result. The sintering densification curve [47] can be calculated according to the following equation:

$$\rho(t,T) = \rho_{gd} * \frac{100^3}{(100 + \epsilon_{tech}(t,T))^3} \tag{3-64}$$

where

- $\rho(t,T)$ - the bulk density or relative density, depending on ρ_{gd}.
- ρ_{gd} - the green density, which is the sample density before sintering and can be measured accurately according to Archimedes' principle (see Appendix C). It can be either bulk density or relative density.

When the sample after sintering doesn't contain open pores. The final density can be measured easier than the green density, and can be more precise. Then the sintering densification curve can be calculated from

$$\rho(t,T) = \rho_f * \frac{(100 + \epsilon_{Tmax})^3}{(100 + \epsilon_{tech}(t,T))^3} \tag{3-65}$$

where

- ρ_f - the final density, which is the sample density after sintering

Here we use equation 3-64. The green ball density[3] is $2.06g/cm^3$ and theoretical density of alumina is 4 g/cm^3. $\rho_{gd} = \frac{2.06g/cm^3}{4g/cm^3} = 0.515$. Then the densification curve is

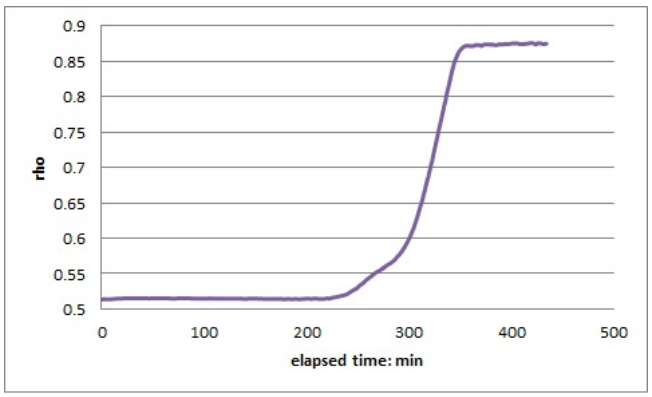

Figure 3-29: Relative Density

The plot of $\ln(TT'\frac{d\rho}{dT})$ vs $\frac{1}{T}$ is

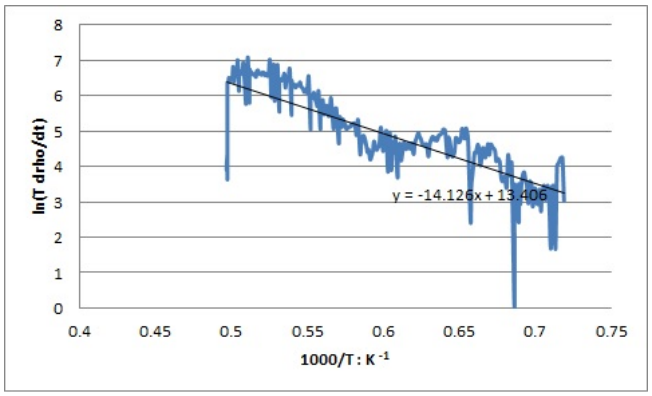

Figure 3-30: $\ln(TT'\frac{d\rho}{dT})$ V.S. $\frac{1}{T}$

The slope -14.12 is equal to $-Q_p/R$, where R is 8.314 $JK^{-1}mol^{-1}$. Then Q_p is $8.314 * 14.12 = 117.39kJ/mol$.

Until now the unknown parameters are k_{p0} and m. The parameter m is related with the diffusion mechanisms and hard to calculate directly. As to the parameter k_{p0}, we also have no idea on how to calculate it. However, if we've already got some experiment data, we can estimate these parameters by trial and error with our model.

[3]The value of green ball density used here is from Almatis website: http://www.almatis.com/.

3-9-4 Model Parameter m and Pre-exponential Parameter k_{p0}

Now we substitute all the values got in the previous discussion into our model. Initial distribution is the log-normal distribution with geometric mean $r_m = 3.747\mu m$ and geometric standard deviation $\sigma = 5.925$. The initial relative density is 0.515. Activation energy for densification is 117.39 kJ/mol.

Compare the results with experiment data using different k_{p0} and m, we can find the proper k_{p0} and m.

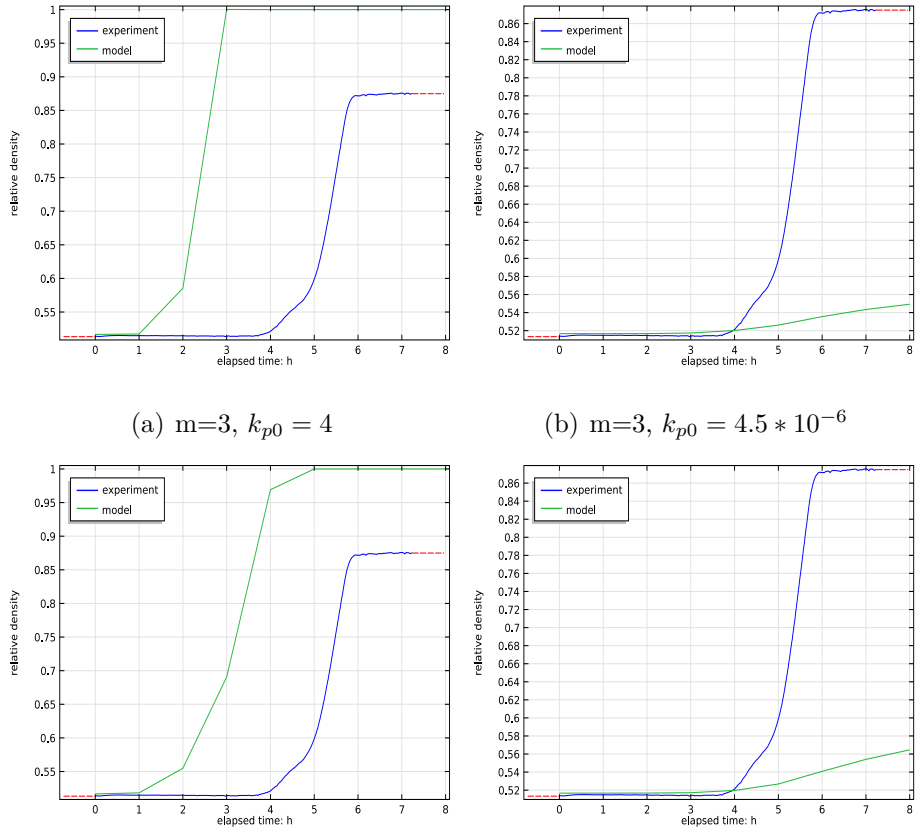

(a) m=3, $k_{p0} = 4$ (b) m=3, $k_{p0} = 4.5 * 10^{-6}$

(c) m=5, $k_{p0} = 4.5 * 10^{-4}$ (d) m=2, $k_{p0} = 4.5 * 10^{-4}$

Figure 3-31: Relative Density: Model V.S. Experiment

When $k_{p0} = 4.5 * 10^{-4}$, $m = 3.4$, the estimation result of the model is closer to that of the experiment data, although there still exists difference.

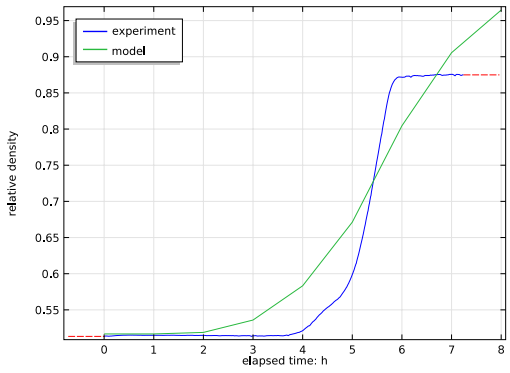

Figure 3-32: Relative Density: Model V.S. Experiment, m=3.4, $k_{p0} = 4.5 * 10^{-4}$

To get a better estimation result, we still have a lot of things to do. First of all, more accurate data about the initial values and other parameters are required. For the initial values, we assume that it fits log-normal distribution. In the real world, initial pore size distribution may not fit very well with log-normal distribution. Use of the original pore size distribution may lead to better estimation result. Even if we accept the log-normal distribution as the initial distribution, more SEM figures are needed to be analyzed, so that the average value can be used. For the green ball density and theoretical density of alumina, more accurate data for different cases from the industry field are necessary, because the feedstock used for different productions may be different. Here the values we used are found via web site. It may be close to but not correspond to the true value. For the dilato test result used to calculate activation energy, it's better to have several set of data using different heating rate but same final temperature, then we can estimate the activation energy in a range. When we calculate the thermal expansion coefficient and relative density, more accurate formula can be used if we can get the corresponding data directly. Besides, it's also possible to adjust our models in some specific cases. For example, we can have several values of m to estimate different part of the densification curve.

If we can get a very close estimation result, we can further try to predict the relative density using our own temperature cycles, which is valuable for production in the industry field.

Chapter 4

Model of Grain Growth

In this chapter we introduce a model for grain growth only. Grain growth describes the increase in the grain size. It occurs in both dense and porous polycrystalline solids at sufficiently high temperatures. For the conservation of matter, the sum of the individual grain sizes must remain constant. So an increase in the average grain size is accompanied by the disappearance of some grains, usually the smaller ones.

The grain growth model has similar structure with the pore shrinkage model. And the structure of this chapter is similar to that of last chapter. However, since the velocity model for grain growth is more complicated, it's hard to get the analytical solution directly. Instead an asymptotic steady-state solutions is used to show that the finite element method using COMSOL 4.3a will lead to a reasonable result.

4-1 Model of grain growth

The continuity equation for the population balance of grain size is [37]:

$$\frac{\partial n_g(r_g,t)}{\partial t} + \frac{\partial}{\partial r_g}(v_{r_g} n_g(r_g,t)) = 0 \tag{4-1}$$

And the velocity function for grain growth is

$$v_{r_g} = \frac{dr_g}{dt} = \frac{k_g}{r_g^n}(\frac{1}{r_c} - \frac{1}{r_g}) \tag{4-2}$$

where r_g (μm) is the grain radius and n_g is the number density function of grain size (which can be got from the histogram of grain size for a given instant in time). k_g ($\mu m^{n+2}/h$) is a function of temperature, diffusivity and surface free energy of the particle material. n (unit:1) is a model parameter which depends on the mechanism of grain growth. r_c (μm) is the critical radius of grain.

From the formula of velocity, we can see that the velocity for grain growth v_{r_g} is negative for $r_g < r_c$, positive for $r_g > r_c$ and zero for $r_g = r_c$. It means that the grains whose radius are smaller than the critical radius are shrinking and those with radius larger than the critical radius are growing. The critical radius is the grain size which neither grow nor shrink at a particular instant of time. For the following figure, the value of critical radius is around 2.5.

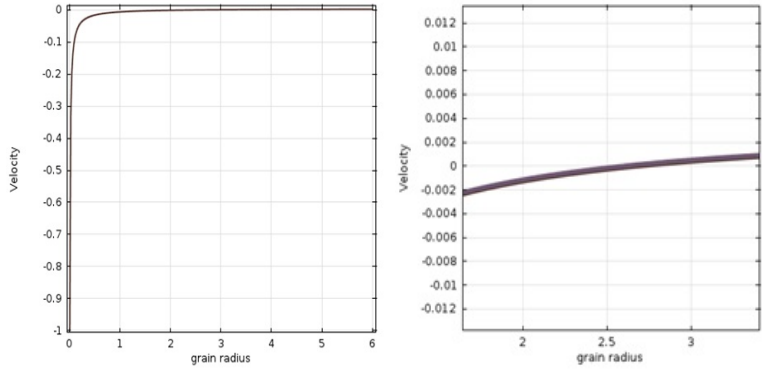

(a) velocity (b) zoom in of left

Figure 4-1: Grain Growth Velocity

4-1-1 The Critial Radius r_c

Since the total volume of particles is conserved during the process, the increased volume of the particles whose size is larger then r_c is equal to the decreased volume of the particles whose size is smaller than r_c, i.e.

$$\Sigma_{i=1}^{N} dr_{g,i}^3 = 0 \tag{4-3}$$

N is the particle number. According to Eq. (5-1),

$$\frac{dr_g}{dt} = \frac{k_g}{r_g^n}(\frac{1}{r_c} - \frac{1}{r_g}) \tag{4-4}$$

$$\Rightarrow \frac{dr_g^3}{dt} = \frac{3r_g^2 k_g}{r_g^n}(\frac{1}{r_c} - \frac{1}{r_g}) \tag{4-5}$$

$$\Rightarrow dr_g^3 = \frac{3r_g^2 k_g}{r_g^n}(\frac{1}{r_c} - \frac{1}{r_g})dt \tag{4-6}$$

$$\Rightarrow \Sigma_{i=1}^{N} dr_{g,i}^{3} = \Sigma_{i=1}^{N} \frac{3k_g}{r_{g,i}^{n-2}} (\frac{1}{r_c} - \frac{1}{r_{g,i}}) dt = 0 \tag{4-7}$$

$$\Rightarrow \Sigma_{i=1}^{N} \frac{1}{r_{g,i}^{n-2}} (\frac{1}{r_c} - \frac{1}{r_{g,i}}) = 0 \tag{4-8}$$

$$\Rightarrow r_c = \frac{\Sigma_{i=1}^{N} r_{g,i}^{2-n}}{\Sigma_{i=1}^{N} r_{g,i}^{1-n}} \tag{4-9}$$

$$\Rightarrow r_c = \frac{\Sigma_{i=1}^{N} r_{g,i}^{2-n}/N}{\Sigma_{i=1}^{N} r_{g,i}^{1-n}/N} \tag{4-10}$$

In case of continuous distribution of particle radius r,

$$r_c = \frac{\int_0^\infty r_g^{2-n} dF(r_g)}{\int_0^\infty r_g^{1-n} dF(r_g)} = \frac{M_{2-n}}{M_{1-n}} \tag{4-11}$$

where $M_k = \int_0^\infty r_g^k dF(r_g) = k \int_0^\infty r_g^{k-1} R(r_g) dr_g$ is the kth moment, $F(r_g)$ is the cumulative distribution function of r_g, and $R(r_g) = 1 - F(r_g)$is the corresponding survival function.

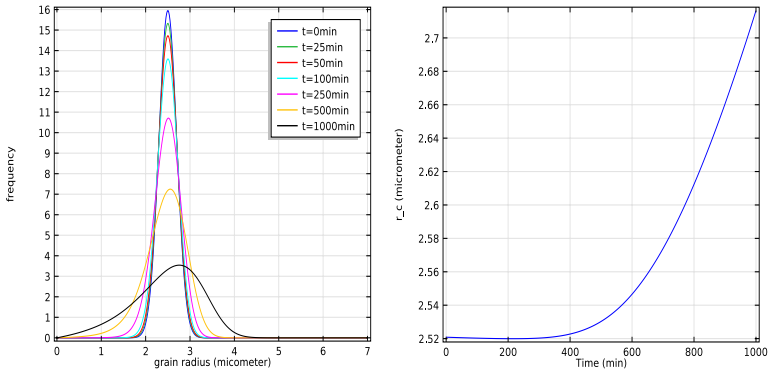

(a) frequency (b) r_c

Figure 4-2: Critical Radius 1

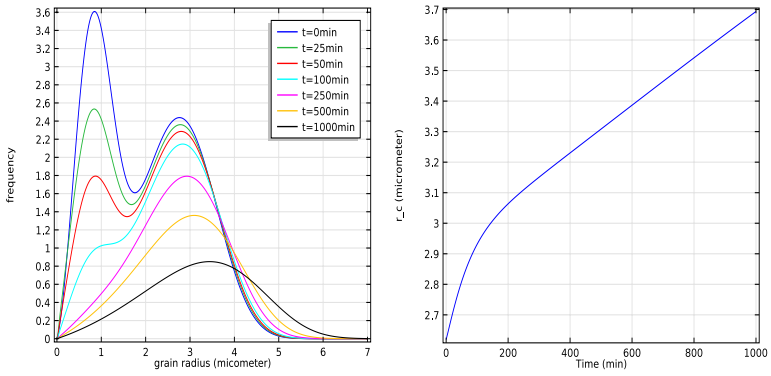

(a) frequency (b) r_c

Figure 4-3: Critical Radius 2

The critical radius r_c is a function of time t. In the case shown in Figure 4-2 where the initial distribution is normal distribution, the value of r_c increases very slowly during the sintering

time. However, we must notice that it doesn't mean r_c is a constant. For example, if we use bimodal distribution, we can see the value of r_c is changing faster in Figure 4-3. This also indicates that the velocity of grain growth is influenced by the initial distribution.

4-1-2 Model Parameter k_g

The model parameter k_g is related with temperature. Similar to k_p in the pore shrinkage model, it's decided by Arrhenius equation (See Appendix E).

$$k_g(T) = k_{g0}e^{-\frac{Q_g}{RT}} \tag{4-12}$$

Where Q_g (unit: J/mol) is the activation energy for grain growth. R (unit: $J \cdot K^{-1}mol^{-1}$) is the gas constant. T (unit: K) is the absolute temperature. The units of the pre-exponential factor k_{g0} is identical to the rate constant k_g and will vary depending on the order of the reaction.

Similar to last chapter, Q_g can be got from experiment data. And k_{g0} can be got from trial and error.

4-1-3 Model Parameter n

For $n = 0$, particle growth is controlled by surface reaction.

For $n = 1$, particle growth is controlled by bulk diffusion.

For $n = 2$, the process of coarsening is limited by diffusion of atoms along grain boundaries.

For $n = 3$, the supply of material to particles is along the cross section dislocation pipes.

If we want to analyze the grain growth process dominated by different diffusion mechanisms separately, we can use n $= 1, 2, 3, 4$. Besides, similar to the parameter m in chapter 3, n can also be non-integer, representing grain growth due to the combination of several diffusion mechanisms.

4-2 Asymptotic Steady-State Solutions

For the case of $n = 0$, the asymptotic steady-sate solution is [49]

$$n_g(u) = n_{g0}u\frac{(\alpha - u)^A}{(\frac{\alpha}{\alpha - 1} - u)^B} \quad 0 \leq u < \alpha \quad and \quad 1.25 \leq \alpha < 2 \tag{4-13}$$

where n_{g0} is a normalizing constant, α the largest u of the function $n_g(u)$, $A = (4\alpha - 5)/(2 - \alpha)$, $B = (5 - \alpha)/(2 - \alpha)$ and $u = \frac{r_g}{r_c}$, $n_g(u) = r_c^4 n_g(r_g)$.

For the case of $n = 1$, the asymptotic steady-sate solution is [50] [51]

$$n_g(u) = n_{g0} \frac{u^2}{(1.5 - u)^{11/3}(3 + u)^{7/3}} e^{\frac{-u}{1.5-u}} \qquad 0 \leq u < 1.5 \tag{4-14}$$

$$n_g(u) = 0 \qquad else \tag{4-15}$$

where n_{g0} is a normalizing constant and $u = \frac{r_g}{r_c}$, $n_g(u) = r_c^4 n_g(r_g)$.

Both of these two solutions are independent with initial grain size distribution.

Take $n = 1$ for example, we use $k_g = 0.01 \mu m^3 min^{-1}$. With different initial grain size distribution, we can see that 'LSW' in the figure is the plot of asyntptotic steady state, to which the numerical solution is getting closer and closer as time going on. It illustrates that the numerical solution is reasonable.

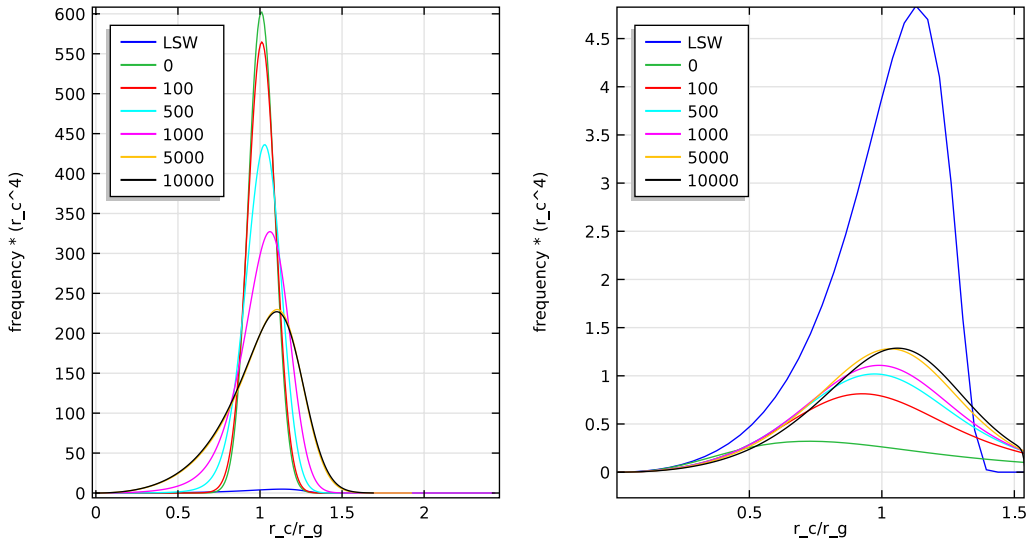

(a) case 1 (b) case 2

Figure 4-4: LSW Solution and Numerical Solution

4-3 Examples and Sensitive Analysis

Here we show an example with parameters from some existing literatures [37]. The initial grain size distribution is Gaussian distribution with mean 2.5 μm and standard deviation 0.2 μm. The other parameter values are $k_g = 0.01 \mu m^2/min, n = 0$.

From Figure 4-5, we can see that the mean grain size is growing over time, that is, grain growth.

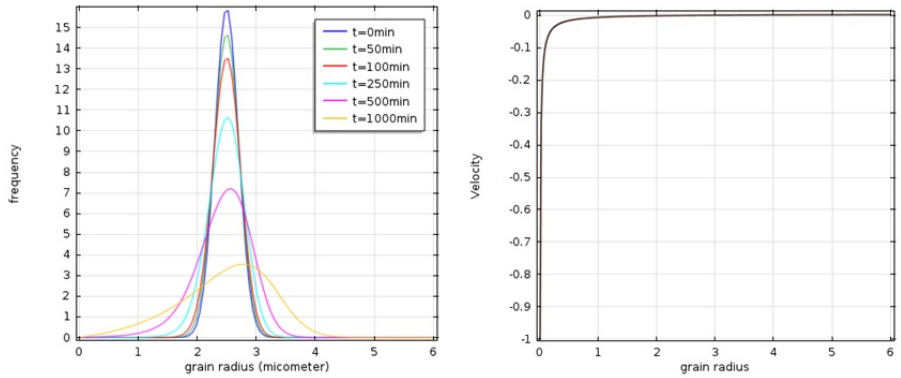

Figure 4-5: Number Density Function of Grain Growth

4-3-1 k_g Change

k_g is a parameter which influences the grain growth velocity both directly and indirectly. It's obvious that k_g will influence the velocity because k_g is one of the parameters which construct the velocity formula. Besides, the value of r_c, another parameter in the velocity model, is also influenced by k_g. So we want to see k_g 's influence on r_c.

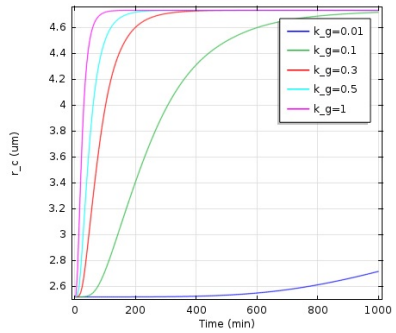

Figure 4-6: r_c Changes with k_g

From Figure 4-6, we can see that in this case, only when k_g is 0.01, r_c is almost a constant. For other values of k_g, r_c is increasing in the beginning and then gets close to a fixed value. So r_c is not a constant, but a function of time t. Recall the definition of r_c, this value depends on the grain size distribution at each time step. When k_g changes, it influences the grain growth velocity and then the grain size distribution at next time step. So r_c will change as well. And then the values of r_c and k_g both contribute to the change of velocity. But k_g contributes more. From Figure 4-7, we can see that although r_c changes a lot, the velocity is not as sensitive as r_c to k_g. For the grains whose size are smaller than r_c, the larger k_g is, the faster shrinkage rate is. But for the grains whose size are larger than r_c, the grain growth rate changing with k_g is not very clear in the figure.

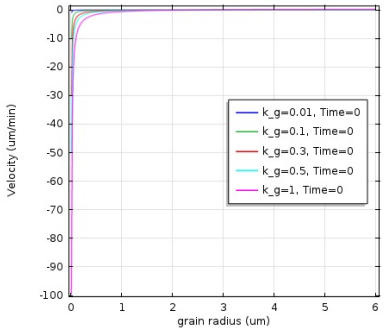

Figure 4-7: Velocity Changes with k_g

Figure 4-8 shows the number density of grain growth changing with k_g. The larger k_g is, the faster the mean grain size increases as time goes on, and the faster the grain number decreases. It can be easily understood. In the beginning of this chapter, we discussed about grain growth. The sum of the individual grain sizes must remain constant, so an increase in the average grain size is accompanied by the disappearance of some grains, usually the smaller ones. From the velocity figure, we know that the larger k_g corresponds to faster shrinkage rate of grains. So more small grains will vanish if k_g is larger. Big grains will grow and won't vanish. So the total number of grains will decrease faster.

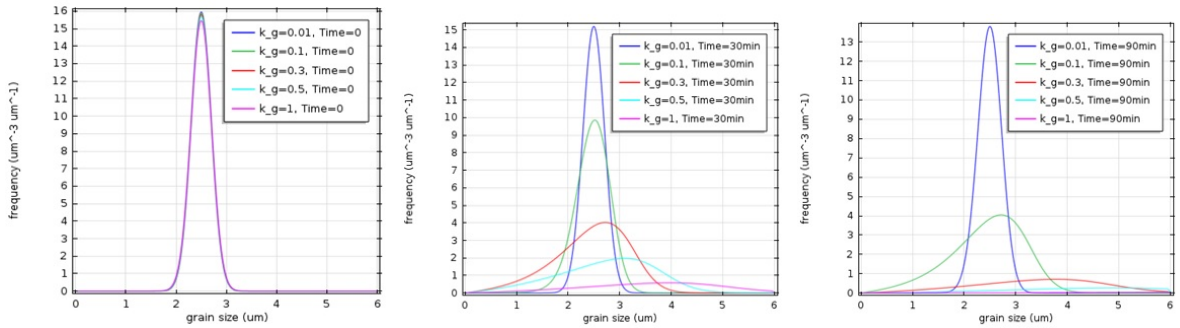

(a) t=0 (b) after 30min (c) after 90min

Figure 4-8: Number Density Function Changing with k_g

4-3-2 n Change

Similar to k_g, n will influence the grain growth velocity both directly and indirectly. But it's hard to say that the critical radius r_c is increasing or decreasing with the change of parameter n.

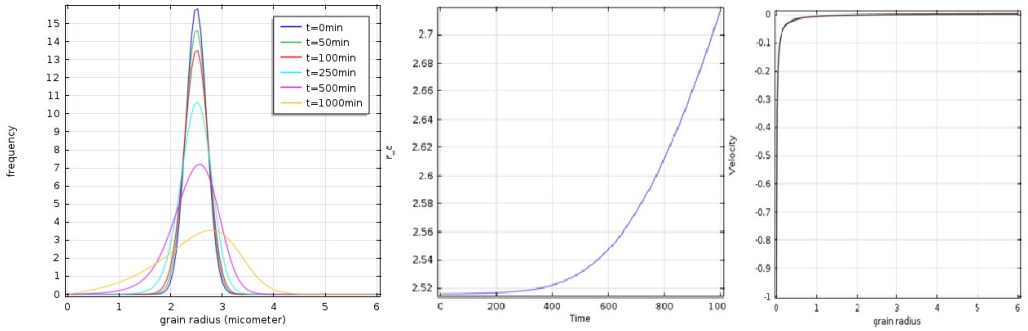

(a) n=0

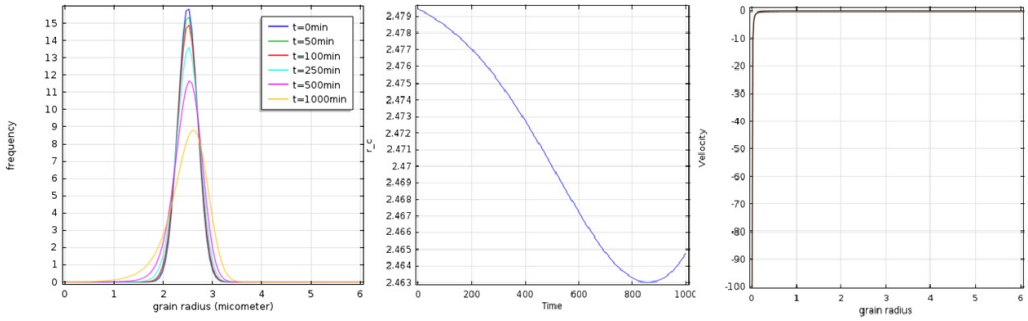

(b) n=1

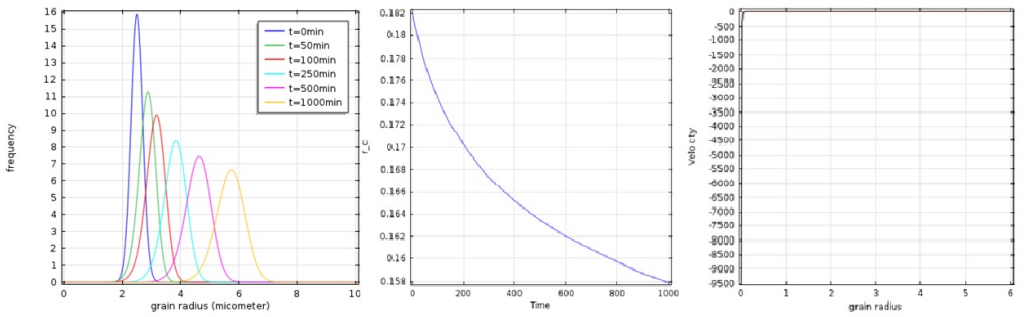

(c) n=2

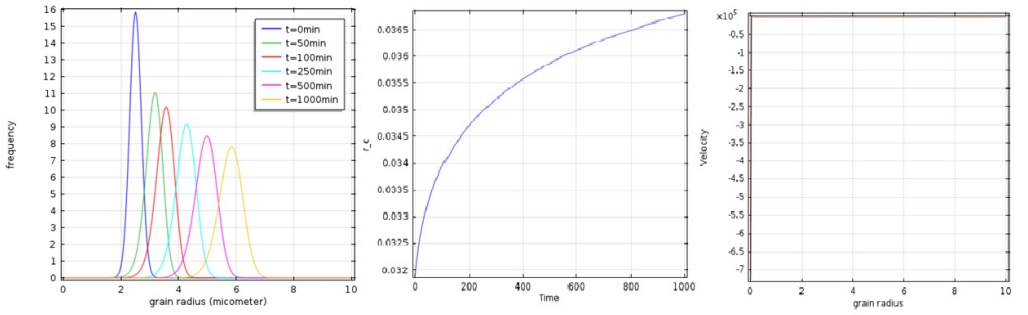

(d) n=3

Figure 4-9: Number Density Function, Critical Radius and Velocity Changing with n

From Figure 4-9, we can see that when n is 0 or 3, the critical radius is an increasing function of time t, and when n is 1 or 2, the critical radius is an decreasing function of time t. The larger n is, the faster the mean grain size increases as time goes on, and the faster the total grain number decreases.

4-3-3 r_c Change and Distribution Change

We won't discuss about the contribution of r_c to the grain growth velocity separately, because r_c won't change itself. It depends on the change of grain size distribution, which is influenced by other parameters. Since r_c is sensitive to the grain size distribution and will influence the velocity, the initial distribution of grains also plays an important role. Figure 4-10 shows two examples with different initial distributions - one is Gaussian distribution and the other is bimodal distribution.

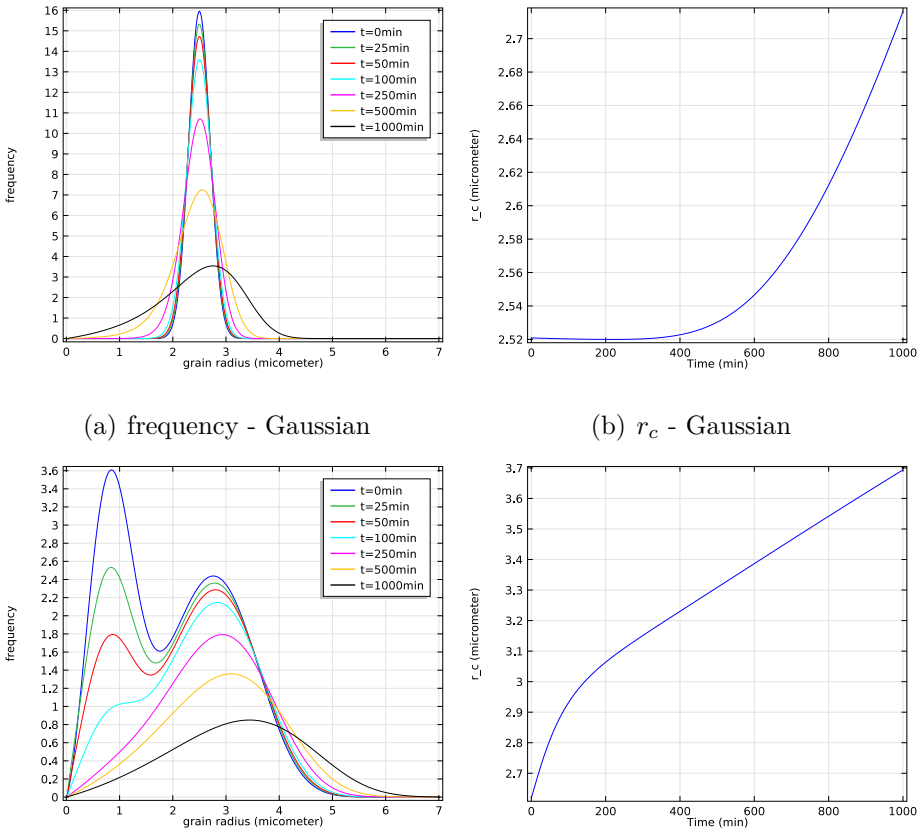

(a) frequency - Gaussian

(b) r_c - Gaussian

(c) frequency - bimodal

(d) r_c - bimodal

Figure 4-10: Number Density of Grain Size with Different Initial Distribution

Chapter 5

Combination of Two Models

In the previous two chapters, we introduced pore shrinkage model and grain growth model separately. In fact, accompanied with the pore shrinkage, porosity (i.e. 1 - relative density) is decreasing and getting close to 0. And porosity could influence the grain growth rate. So the porosity could be added into the velocity model of grain growth, so as to get a coupled model.

5-1 Coupled Model

The two models are combined with parameter relative density ρ. It can be calculated from the result of pore shrinkage model and then be considered as an input parameter for the grain growth model.

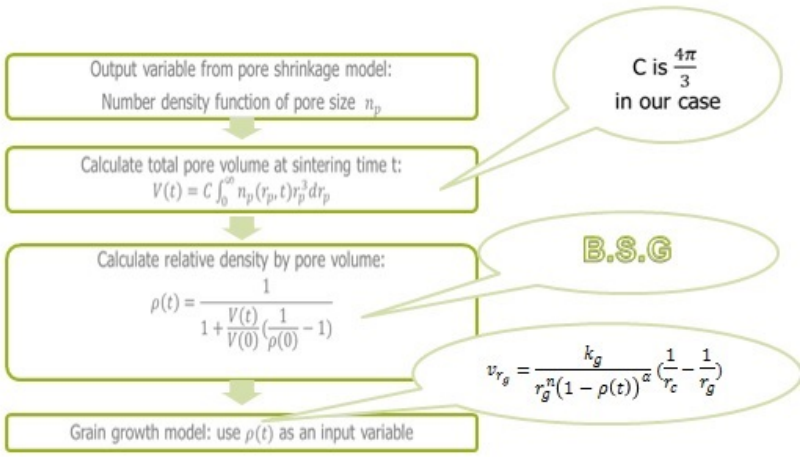

Figure 5-1: Flowchart of Combination Model

The velocity model for isolated grain growth in last chapter is changed to [37]

$$v_{r_g} = \frac{dr_g}{dt} = \frac{k_g}{r_g^n(1-\rho(t))^\alpha}(\frac{1}{r_c} - \frac{1}{r_g}) \tag{5-1}$$

where $\rho(t)$ (unit: 1) is the relative density and α (unit: 1) is a model parameter. Other parameters in the formula have the same explanation as those in last chapter. This is the velocity model for grain growth coupled with densification.

When the porosity $(1-\rho)$ is getting close to 0, the grain growth rate is becoming larger; when the porosity is getting close to 1, the grain growth rate is becoming smaller. This phenomenon is understandable because when porosity is 0, there is no pore inside the material, grains are next to each other, it's very convenient for combination of grains.

Due to lack of experiment data, we don't get our own parameter values. Here we use the parameter values from Pradip's work [37] and others' work to show an example. Assume that the initial distribution of pore size is log-normal with median size $0.034\mu m$ and geometric standard deviation 1.2 and initial distribution of grain size is log-normal with median size $0.98\mu m$ and geometric standard deviation 2. $m = 6, k_p = 1.00 * 10^{-13}\mu m^7/h, n = 4, \alpha = 1, k_g = 0.06\mu m^6/h, \rho(0) = 0.42$. The results are shown as follows:

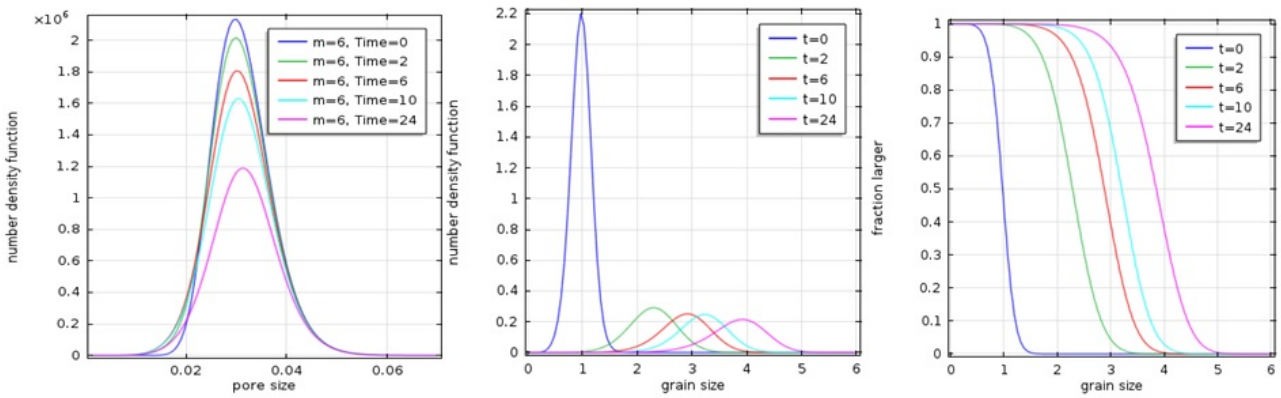

Figure 5-2: Combination Model Results

5-2 Sensitive Analysis

5-2-1 m Change

Change of m will first influence the pore shrinkage model, and further the relative density and grain growth model. Sensitive analysis of m to the pore shrinkage model has been discussed in Chapter 3, and can be seen in Figure 5-3.

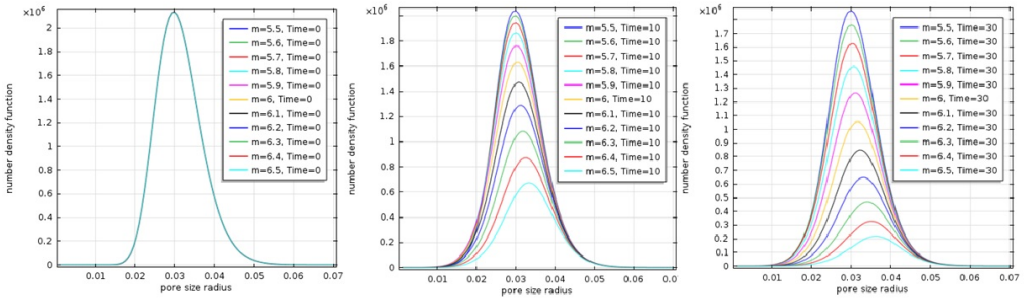

Figure 5-3: Pore Size Distribution Changing with m

The relative density is increasing with time. When m increases, the increase rate of relative density is getting faster. The total pore volume is decreasing with time. When m increases, the decrease rate of total pore volume is getting faster (see Figure 5-4).

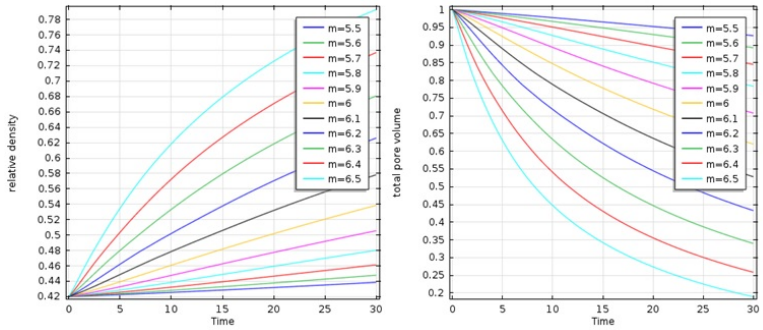

Figure 5-4: Relative Density and Total Pore Volume Changing with m

Similar to what we discussed in last chapter, except for the influence on velocity directly, changing of relative density $\rho(t)$ will also influence the value of r_c (see Figure 5-5). In this case the critical radius r_c and the velocity of grain growth are not sensitive to small change of m. We can imagine that the grain size distribution is not sensitive to m. This is illustrated in Figure 5-6.

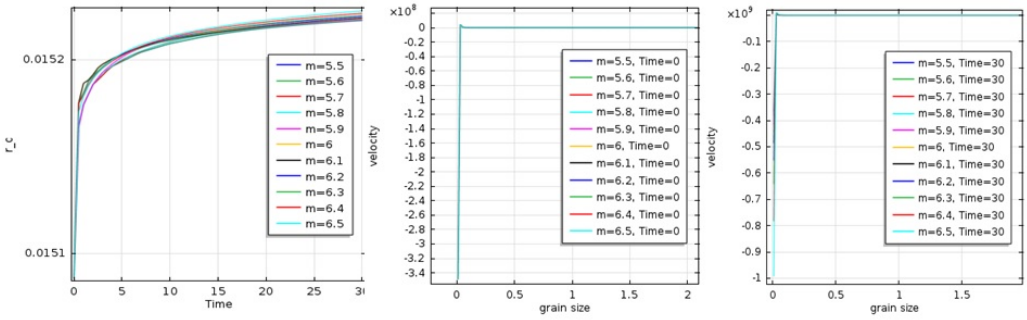

Figure 5-5: Critical Radius Changing with m

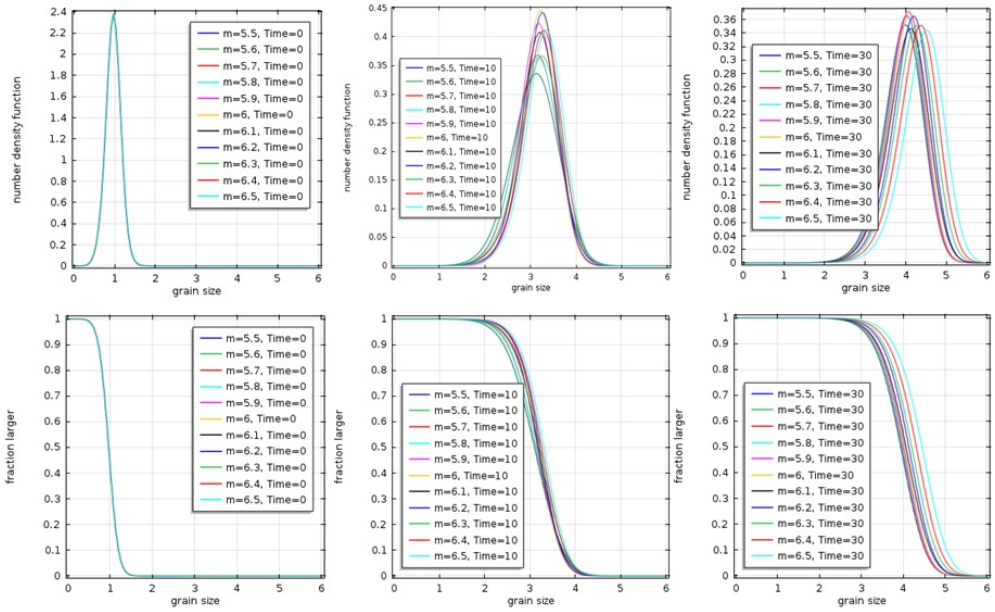

Figure 5-6: Grain Size Distribution Changing with m

5-2-2 k_p Change

Similar to m, the influence on pore size distribution by changing k_p has been discussed in Chapter 3. It can be seen from Figure 5-7.

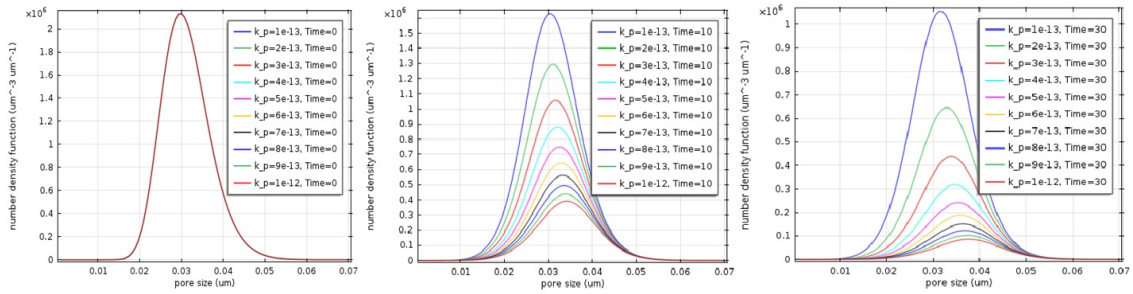

Figure 5-7: Pore Size Distribution Changing with k_p

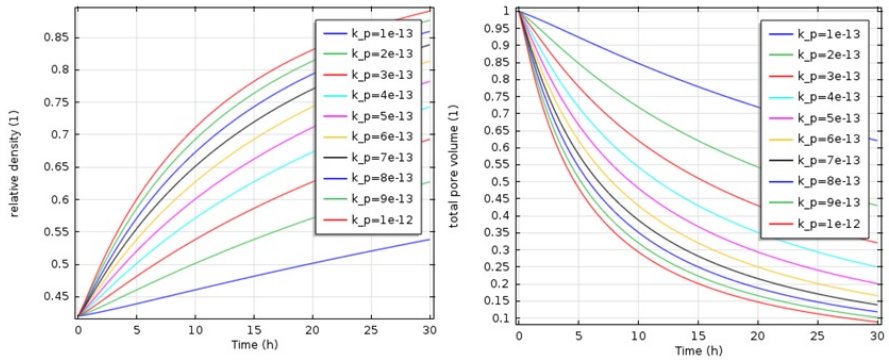

Figure 5-8: Relative Density Changing with k_p

From Figure 5-8, the relative density is increasing with time. When k_p increases, the increase

rate of relative density is getting faster. The total pore volume is decreasing with time. When k_p increases, the decrease rate of total pore volume is getting faster.

In this case the critical radius r_c and the velocity of grain growth at each time point are not sensitive to small change of k_p (see Figure 5-9). The grain size distribution is not sensitive to k_p, either (see Figure 5-10).

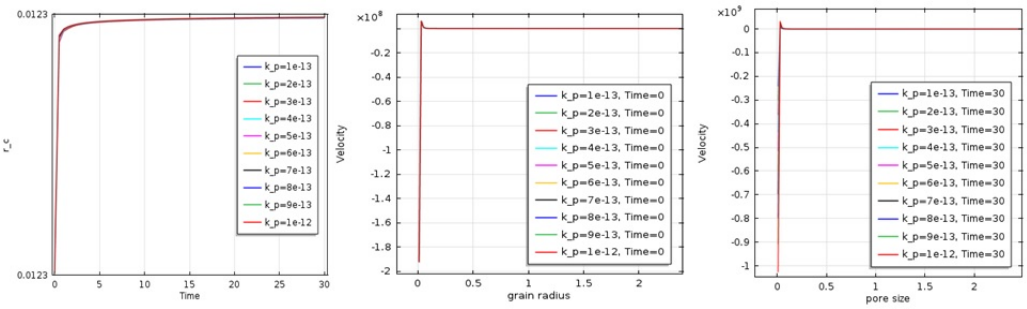

Figure 5-9: Critical Radius Changing with k_p

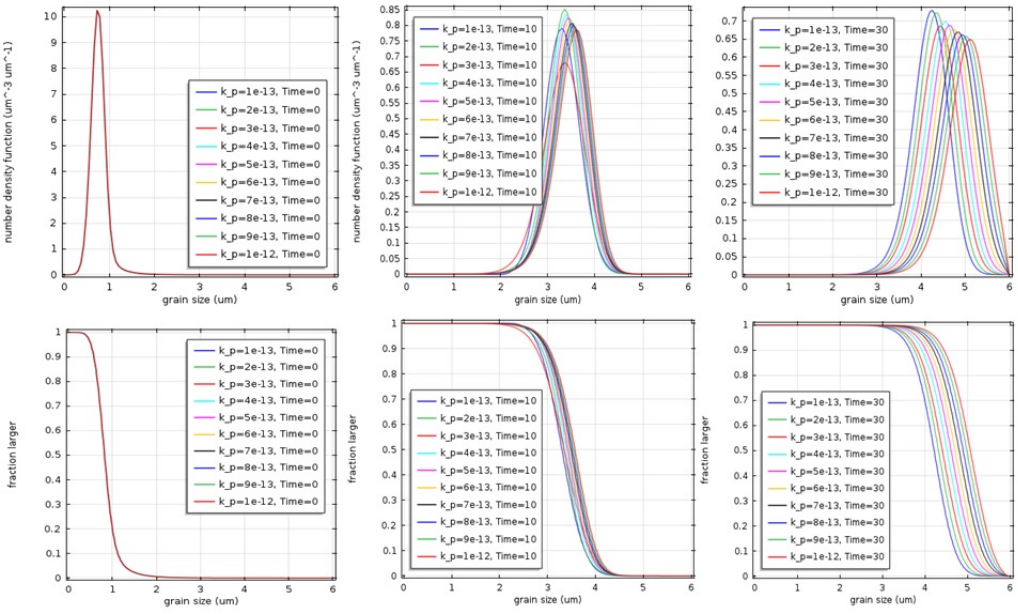

Figure 5-10: Grain Size Distribution Changing with k_p

5-2-3 k_g Change

We can see that in this case changing the value of k_g won't influence the value of critical radius r_c too much. And the grain size distribution is not sensitive to k_g.

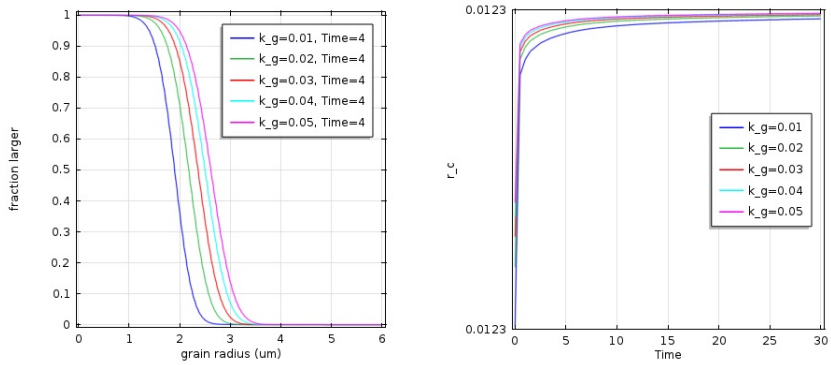

Figure 5-11: Grain Size Distribution Changing with k_g

5-2-4 α Change

We can see that in this case changing the value of α 's influence on the value of critical radius r_c contributes more than above parameters, and further contributes more on the final results.

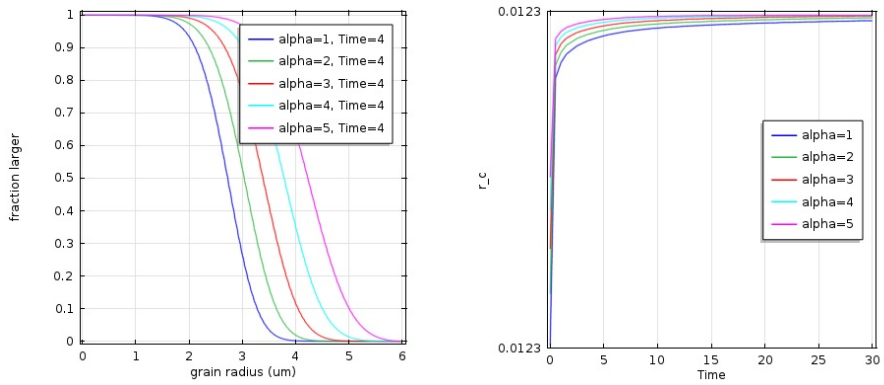

Figure 5-12: Grain Size Distribution Changing with α

5-2-5 n Change

n is a parameter corresponding to the material transport mechanism. We can see that different transport mechanism will lead to different results. When n is changing from 0 to 2, the difference is not clear. But when n is changed to 3, the result is apparently different from the others.

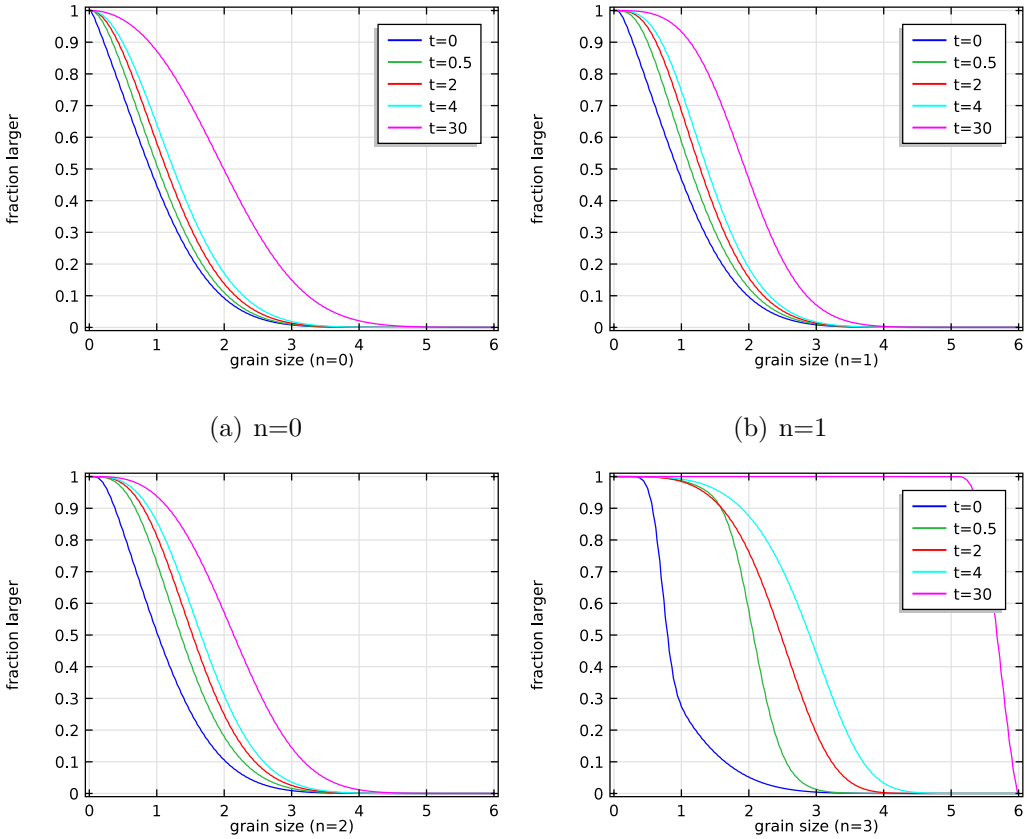

(a) n=0 (b) n=1

(c) n=2 (d) n=3

Figure 5-13: Grain Size Distribution Changing with n

Above all, in this case n plays the most important role in the combination model. k_g and α are less important. Parameters m and k_p, which exists in the pore shrinkage model, although having relatively significant influent on the relative density, are not as important as parameters directly existing in the combination model, i.e. k_g, α and n. However, sensitive analysis might be different from cases.

Chapter 6

Application in Industry Field

In the above examples, we consider all the parameters as a constant. However, in the real world, the temperatures are changing over time. And the corresponding parameters k_p and k_g are influenced by temperature. Generally, these two parameters are decided by Arrhenius equation (See Appendix E).

$$k_p(T) = k_{p0} exp(-\frac{Q_p}{RT}) \tag{6-1}$$

$$k_g(T) = k_{g0} exp(-\frac{Q_g}{RT}) \tag{6-2}$$

Parameters we used are as follows [37]:

$m = 4, k_{p0} = 1.9879e+005, Q_p = 131kJ/mol;\ n = 2, k_{g0} = 8.7720e+011, Q_g = 533kJ/mol$

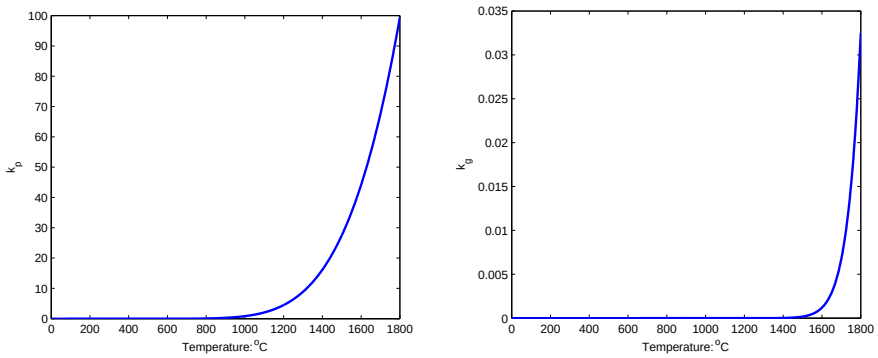

(a) k_p *V.S.* T (b) k_g *V.S.* T

Figure 6-1: k_p vs T and k_g vs T

First we start with an simple example. Initial pore size distribution is supposed to be log-normal with $r_m = 0.034\mu m, \sigma = 1.2$. The temperature increases in the first two hours and then is kept in a constant level. The relative density is increasing as well, slowly in the beginning but faster in the next 4 hours.

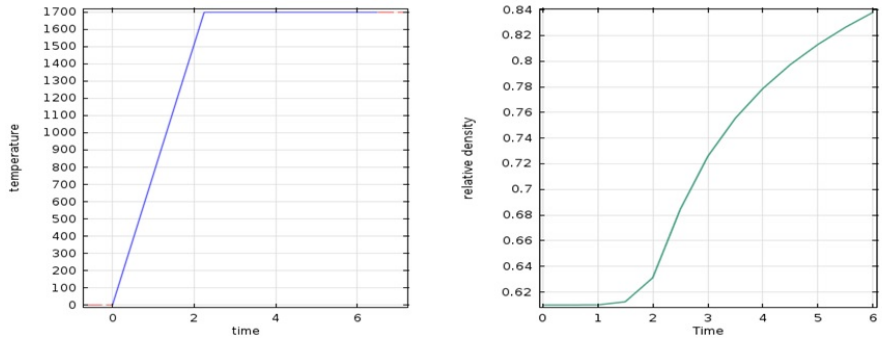

Figure 6-2: Application 1

The second example is about three similar temperature cycles. Initial pore size distribution is supposed to be log-normal with $r_m = 4\mu m, \sigma = 1.4$. In the first 4 hours, temperature is increasing to 800 °C linearly. While in the following 2 hours the temperature increasing rates are different. Then the corresponding relative density increasing rate are also different. Faster heat up rate leads to faster increasing rate of relative density.

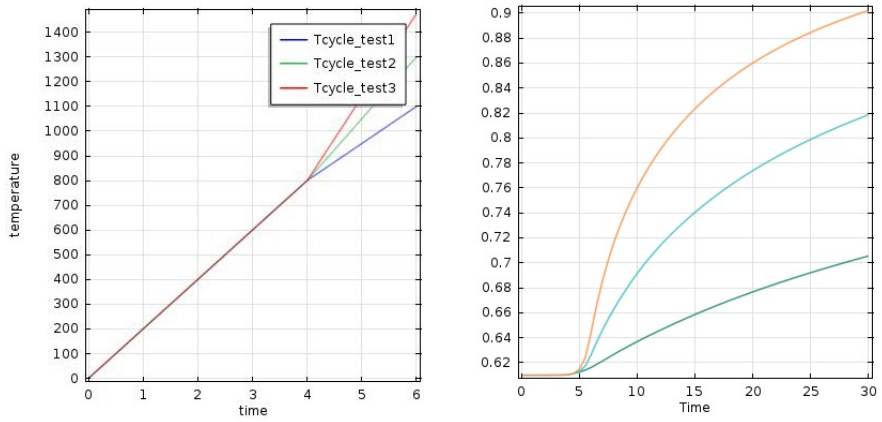

Figure 6-3: Application 2

The third example is temperature cycles which increase fast in the beginning, keeps almost constant for a while, and then decrease slowly.

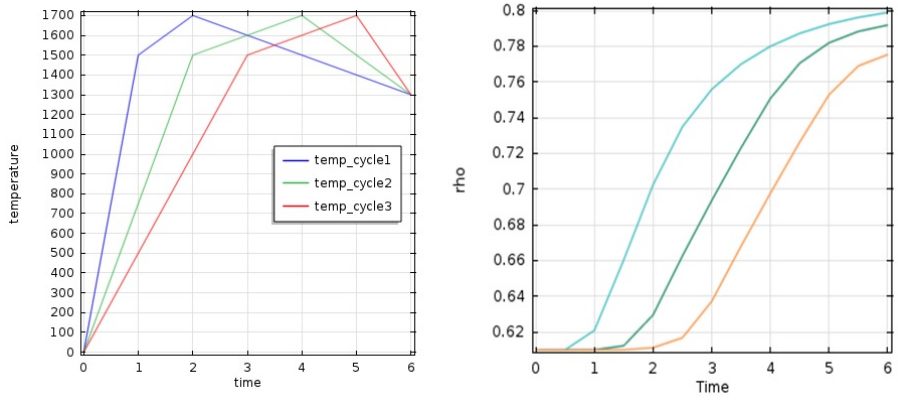

Figure 6-4: Application 3

This kind of temperature cycle can be got from the combustion model of shaft kiln, since the temperature increases in the preheating zone, and decreases in the cooling zone.

Chapter 7

Conclusion and Future Work

In this project we focus on the sintering process of making tabular alumina from α-alumina. The main work is based on M. Subbanna, P.C. Kapur, Pradip, S.G. Malghan's models built in 2000. To make problem simple, we only consider solid state sintering, which includes pore shrinkage process and grain growth process. In general, these two processes happen simultaneously. However, lots of literatures have shown that pore shrinkage may be analyzed independent of grain growth. So in our model, pore shrinkage is analyzed independently. Then the results of pore shrinkage model is embedded into the grain growth model. The coupling of pore shrinkage and grain growth is through the relative density which depends on the solution of the pore shrinkage model.

The theoretical basis of both of the two models are continuity equation. Here we solve the PDEs using finite element method (streamline-diffusion method) with COMSOL Multiphysics 4.3a. The reason we choose COMSOL Multiphysics to solve this problem is that we want to use the estimated temperature cycle which comes from the combustion model[1] in the future. For the pore shrinkage model, we use analytical solution and solution generated using finite different method in Matlab to verify that FEM can generate a 'good' result as well. For the grain growth model which is a little bit more complicated, it's hard to get the analytical solution directly. We use asymptotic steady-state solutions instead to verify the FEM solution.

One important use of the pore shrinkage model is to estimate the relative density (also called bulk specific gravity, i.e. BSG). The initial pore size distribution can be got from image analysis

[1]This is another project in Almatis, which would simulate the temperature distribution in the shaft kiln.

method with software Image J. Activation energy can be estimated from the Dilato test result. And other model parameters can be estimated by trial and error using the Dilato test result. We use the feedstock KA-13 in Ludwigshafen as an example. Comparison between experiment data and the simulation result shows that our model is reasonable.

However, the estimation result is not as good as we expect. There are lots of factors which would influence the result. First, the image analysis process we used to estimate initial pore size distribution is not so accurate. Figures with larger amplification factor may be more helpful. And it's better to analyze enough figures and then find the average value. Secondly, we assume that the initial pore size distribution fits log-normal distribution. In the real world, initial pore size distribution may not fit very well. Thirdly, when calculating activation energy, it's also better to use data from several Dilato tests with different temperature cycles and then to find the range of activation energy for pore shrinkage. Besides, some parameter values we used for simulation are found via web site. If we can test these values by ourselves using the corresponding product, results may be better. There are also some parameters hard to be calculated directly. So we have to use trial and error method to estimate these values. Maybe in the future we can try to look for some other methods to calculate these parameters.

For isolated grain growth model and the combination model, it's a pity that until now we haven't got our own examples due to lack of information. This part is really interest in the future.

And to make problem simple, we made lots of assumptions, which are different from that in the real world. For example, the temperature cycle we used in the last chapter is very simple and may be far away from the real world. Data from the combustion model (which is another project in Almatis B.V.) may provide us more reasonable values. More realistic results are expected in the future.

Furthermore, it's also possible to expand the 1D model to 2D or even 3D in COMSOL, so that people can see clearly what has happened during the sintering process.

Chapter 8

The Back of the Thesis

Appendices are found in the back.

8-1 Appendix A - Particles [1]

All the materials in the world are either crystalline or amorphous (or glassy) in structure. A primary particle is a discrete, low-porosity unit that can be either a single crystal, a polycrystalline particle, or a glass. If any pores are present, they are isolated from each other. In this report the primary particle is defined as the smallest unit in the powder with a clearly defined surface.

Normally, crystalline ceramics (and metals) are actually polycrystalline - they are made up of a large number of small crystals, or grains, separated from one another by grain boundaries.

An agglomerate is a cluster of primary particles held together by surface forces, by liquid, or by a solid bridge.

Particles can consist of primary particles, agglomerates, or some combination of the two. They are small units that move as separate entities when the powder is dispersed by agitation.

In ceramics as well as in metals, we focus on both of the atomic scale structure and the microstructure. For the atomic scale: the research is about the type of bonding and the crystal structure (for a crystalline ceramic) or the amorphous structure (if it is glassy). As to the microstructure, if refers to the nature, quantity, and distribution of the structural elements or phases in the ceramic (e.g., crystals, glass, and porosity).

8-2 Appendix B - Log-normal Distribution

The normal distribution is the most common used distribution. It can be expressed in terms of mean $\bar{x}$ and standard deviation σ_x. The density function is

$$n(x) = \frac{dN}{dx} = \frac{1}{\sqrt{2\pi}\sigma_x} e^{-\frac{1}{2}(\frac{x-\bar{x}}{\sigma_x})^2} \tag{8-1}$$

where

$$\bar{x} = \frac{\Sigma x_i \Delta N_i}{\Sigma \Delta N_i} \tag{8-2}$$

Since there is no limitation for the values of x, x can be both positive and negative, which sometimes doesn't fit the reality. For example, the particle size can only be positive. So we substitute $x = lnD$ into 8-1 (which maps $x \in [-\infty, \infty]$ to $D \in [0, \infty]$) and get

$$n(lnD) = \frac{dN}{dlnD} = \frac{1}{\sqrt{2\pi}\sigma_g} e^{-\frac{1}{2}(\frac{lnD-ln\tilde{D}}{\sigma_g})^2} \tag{8-3}$$

where σ_g and $\tilde{D}$ are to be defined.

Since $dlnD = D^{-1}dD$,

$$n(D) = \frac{dN}{dD} = \frac{dN}{DdlnD} = \frac{1}{\sqrt{2\pi}D\sigma_g} e^{-\frac{1}{2}(\frac{lnD-ln\tilde{D}}{\sigma_g})^2} \tag{8-4}$$

which is the common form of log-normal distribution.

Geometric mean:

$$ln\tilde{D} = \frac{\Sigma lnx_i \Delta N_i}{\Sigma \Delta N_i} \tag{8-5}$$

Geometric standard deviation:

$$(ln\sigma_g)^2 = \frac{\Sigma (ln\frac{x_i}{\bar{x}})^2 \Delta N_i}{\Sigma \Delta N_i} \tag{8-6}$$

8-3 Appendix C - Archimedean Principle

The Archimedean principle is named after its discoverer, Archimedes of Syracuse. This principle says that when a body is partly or totally immersed in a fluid there is an upthrust that is equal to the weight of fluid displaced. It's easy to use this principle to calculate the density of materials.

Consider a simple case: an object hanged on a string is immersed in a container of water, as depicted in the following. Because the object is in static equilibrium, the net force on the object is zero, i.e. $W_a + B - W = 0$. where

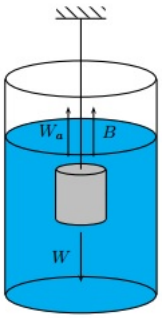

Figure 8-1: Archimedean Principle

- W_a is the apparent weight of the object
- B is the buoyant force, $B = \rho_{water} g V_{water}$, g is the gravity of earth
- $W = M_{obj} g$ is the weight of the object, M is the mass of the object

Then $\rho_{obj} = \frac{M_{obj}}{V_{obj}} = \frac{M_{obj}}{V_{water}} = \frac{M_{obj}}{B/(\rho_{water} g)} = \frac{M_{obj}}{M_a - M_{obj}} * \rho_{water}$, where $M_a = W_a/g$.

8-4 Appendix D - Stoke's Law

In 1851, George Gabriel Stokes derived an expression, known as Stokes' law, for the frictional force exerted on spherical objects with very small particles in a continuous viscous fluid [52].

$$F_d = 6\pi\mu R u \tag{8-7}$$

where

- F_d - the friction force (unit: N)
- μ - the dynamic viscosity (unit: Ns/m^2)
- R - the radius of the spherical object (unit: m)
- u - the particle's velocity (unit: m/s)

8-5 Appendix E - Arrhenius Equation[2]

8-5-1 Reaction Rate Constant

For a chemical reaction where two substances A and B are reacting to produce C.

$$A + B \rightarrow C \tag{8-8}$$

Assume that at least one of them (i.e. A) is in a form where it is sensible to measure its concentration - for example, in solution or as a gas. we could measure the rate of the reaction by finding out how fast the concentration of A was falling per time period. The reaction rate is as follows:

$$r = k[A]^m[B]^n \tag{8-9}$$

This is called the rate equation for the reaction. r represents the reaction rate (unit: $mol \cdot L^{-1} \cdot s^{-1}$). [A], [B] are respectively the concentration of substance A and substance B in moles per volume of solution (unit: $mol \cdot L^{-1}$). m and n are called partial orders and depend on the reaction mechanism (unit: 1). They can be determined experimentally. k is the reaction rate constant. The unit of k depends on the global partial orders (m+n) (unit: $mol^{1-(m+n)} \cdot L^{(m+n)-1} \cdot s^{-1}$).

The rate equation shows the effect of changing the concentrations of the reactants on the rate of the reaction. But other things (like temperature and catalysts, for example) also change rates of reaction. Where do these fit into this equation? These are all included in the rate constant k - which is only actually constant if all you are changing is the concentration of the reactants. If you change the temperature or the catalyst, for example, the rate constant will change.

This can be shown in the Arrhenius equation.

8-5-2 Arrhenius Equation

Arrhenius Equation was proposed by Svante Arrhenius in 1889. It is a simple but useful equation to show the dependence of the rate constant k of chemical reactions on the temperature T.

$$k = k_0 e^{-\frac{Q}{RT}} \tag{8-10}$$

where k is the reaction rate constant discussed in last section. T is the temperature (to fit into the equation, T has to be meaured in kelvin, unit: K). R (unit: $J \cdot mol^{-1} \cdot K^{-1}$) is the gas constant coming from the equation, $pV = nRT$, which relates the pressure, volume and temperature of a particular number of moles of gas. Q (unit: $J \cdot mol^{-1}$) is the activation energy, which is the minimum energy needed for the reaction to occur. The pre-exponential factor k_0 (unit: same as k) is is a term which includes factors like the frequency of collisions and their orientation.aries slightly with temperature, although not much. It is often taken as constant across small temperature ranges.

The Arrhenius eqaution can be also written as

$$lnk = lnk_0 - \frac{Q}{RT} \tag{8-11}$$

The graph between ln k and $1/T$ is a straight line with an intercept of $ln(k_0)$ and the slop of the graph is equal to $-Q/R$.

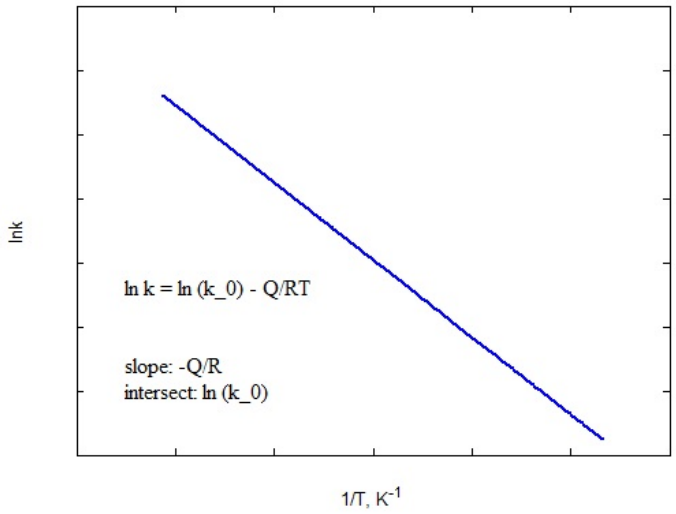

Figure 8-2: Arrhenius Plot

Bibliography

[1] M. N. Rahaman, *Ceramic Processing and Sintering*. Second Edition ed.

[2] K. J. Laidler, *Chemical Kinetics, 3/e*. Pearson Education India, 1987.

[3] http://img.alibaba.com/photo/206040718/2.jpg

[4] http://www.alteo-alumina.com/en/gardanne

[5] K. Wefers and C. Misra, "Oxides and hydroxides of aluminum.(report)," *Aluminum Company of America, 92*, p. 1987, 1987.

[6] http://en.wikipedia.org/wiki/File:Corundum.GIF

[7] K. Amthauer, A. Buhr, M. Schnabel, S. Freundlich, D. Schmidtmeier, and J. Dutton, "New european sinter aggregate with 96% al2o3," in *54th Intern. Colloq. Refractories*, pp. 19–20, 2011.

[8] Suk-Joong L. Kang, *Sintering: Densification, Grain Growth and Microstructure*. Butterworth-Heinemann, 2005.

[9] http://www.thermopedia.com/content/906/

[10] H. Tanaka, A. Yamamoto, J.-i. Shimoyama, H. Ogino, and K. Kishio, "Strongly connected ex situ mgb2 polycrystalline bulks fabricated by solid-state self-sintering," *Superconductor Science and Technology*, vol. 25, no. 11, p. 115022, 2012.

[11] "Dilatometry method, instruments, applications,"

[12] Š. Valovič and I. Štubňa, "Calibration of the horizontal pushrod dilatometer," in *Proc. of the Meeting of the Thermophysical Society-Working Group of the Slovak Physical Society THERMOPHYSICS 2002*, 2002.

[13] F. A. Dullien, *Porous media: fluid transport and pore structure*. Access Online via Elsevier, 1991.

[14] A. Ern and J. Guermond, "Theory and practice of finite elements, volume 159 of applied mathematical series," 2004.

[15] A. J. Downs, *Chemistry of aluminium, gallium, indium, and thallium*. Springer, 1993.

[16] Z. Luo and A. Soria, "Prospective study of the world aluminium industry," *JRC Scientific and Technical Reports. EUR*, vol. 22951, 2007.

[17] http://bauxite.world-aluminium.org/refining/process.html

[18] J. M. Andersson, *Controlling the formation and stability of alumina phases*. PhD thesis, Jönköping University, 2005.

[19] K. Morrissey, K. Czanderna, R. Merrill, and C. Carter, "Transition alumina structures studied using hrem," *Ultramicroscopy*, vol. 18, no. 1, pp. 379–385, 1985.

[20] G. Rankin and H. Merwin, "The ternary system cao-al2o3-mgo.," *Journal of the American Chemical Society*, vol. 38, no. 3, pp. 568–588, 1916.

[21] F. Cardarelli, *Materials handbook: a concise desktop reference*. Springer, 2008.

[22] G.Buchel, X.Liu, A.Buhr and J.Dutton, "Review of Tabular Alumina as High Performance Refractory Material," 2007.

[23] http://alteo-alumina.com/en/aluminas

[24] C. Herring, "Effect of change of scale on sintering phenomena," *Journal of Applied Physics*, vol. 21, no. 4, pp. 301–303, 1950.

[25] F. Rhines and R. T. DeHoff, "Channel network decay in sintering," in *Materials Science Research*, pp. 49–61, Springer, 1984.

[26] G. Kuczynski, "Statistical theory of sintering," *Zeitschrift fuer Metallkunde*, vol. 67, pp. 606–610, 1976.

[27] http://www.serviquimia.com/upload/documentos/20110311134158.dilatometros.pdf

[28] C. Zender, "Particle size distributions: Theory and application to aerosols, clouds, and soils." 2010.

[29] F. A. Dullien and V. Batra, "Determination of the structure of porous media," *Industrial & Engineering Chemistry*, vol. 62, no. 10, pp. 25–53, 1970.

[30] J. G. J. Peelen, *Alumina: sintering and optical properties*. PhD thesis, Technische Hogeschool Eindhoven, 1977.

[31] T.-S. Yeh and M. D. Sacks, "Effect of particle size distribution on the sintering of alumina," *Journal of the American Ceramic Society*, vol. 71, no. 12, pp. C–484, 1988.

[32] T. AEH, "A text-book of mineralogy: With an extended treatise on crystallography and physical mineralogy," *Nature*, vol. 110, p. 210, 1922.

[33] J. A. Schetz and A. E. Fuhs, *Fundamentals of fluid mechanics*. John Wiley & Sons, 1999.

[34] Randolph A. D. and Larson M. A., *Theory Of Particulate Processes*. Academic Press, 1971.

[35] P. K. S. Sivakumar, Pradip and M. S.G, "A size interval-by-size interval marching algorithm for modelling grain growth in the intermediate stage of sintering," vol. 13, no. 1, pp. 173–182(10), 1998.

[36] Manjunath Subbanna, P.C. Kapur, Pradip and S.G. Malghan, "Population balance model for solid state sintering I. Pore Shrinkage and densification," *Ceramics International*, vol. 27, no. 1, pp. 57 – 62, 2001.

[37] S. Sivakumar, Manjunath Subbanna, Satyam S. Sahay, Vijay Ramakrishnan, P.C. Kapur, Pradip, and S.G. Malghan, "Population balance model for solid state sintering II. Grain growth," *Ceramics International*, vol. 27, no. 1, pp. 63 – 71, 2001.

[38] COMSOL, *COMSOL Multiphysics Reference Manual*, comsol 4.3b ed., 5 2013.

[39] Fred Vermolen, *Introduction into Finite Elements*.

[40] T.-P. Fries and H. G. Matthies, "A review of petrov–galerkin stabilization approaches and an extension to meshfree methods," *Institute of Scientific Computing, Univ. of Braunschweig–Inst. of Technology, TR-2004-01, Brunswick, Germany*, 2004.

[41] http://rsbweb.nih.gov/ij/docs/intro.html

[42] R. O. Grubel, "Metallurgy of elemental and compound semiconductors(proceedings of a technical conference...)," in *Metallurgical society conferences*, Interscience publishers, 1961.

[43] A. G. Evans and F. A. Leckie, "The processing and mechanical properties of high temperature/high performance composites. book 5. processing and miscellaneous properties," tech. rep., DTIC Document, 1993.

[44] S. Lopez, S. Yobanny, J. Serrato Rodriguez, and S. Sugita Sueyoshi, "Determination of the activation energy for densification of porcelain stoneware," *Journal of Ceramic Processing Research*, vol. 12, no. 3, pp. 228–232, 2011.

[45] J. Wang and R. Raj, "Estimate of the activation energies for boundary diffusion from rate-controlled sintering of pure alumina, and alumina doped with zirconia or titania," *Journal of the American Ceramic Society*, vol. 73, no. 5, pp. 1172–1175, 1990.

[46] W. S. Young and I. B. Cutler, "Initial sintering with constant rates of heating," *Journal of the American ceramic Society*, vol. 53, no. 12, pp. 659–663, 1970.

[47] K. Maca, V. Pouchly, and A. Boccaccini, "Sintering densification curve: A practical approach for its construction from dilatometric shrinkage data," *Science of Sintering*, vol. 40, no. 2, pp. 117–122, 2008.

[48] C. Y. Ho and R. E. Taylor, *Thermal expansion of solids*, vol. 4. ASM international, 1998.

[49] H. Oel, "Crystal growth in ceramic powders.," tech. rep., Max Planck Institut fuer Silikatforschung, Wuerzburg, Ger., 1969.

[50] I. M. Lifshitz and V. V. Slyozov, "The kinetics of precipitation from supersaturated solid solutions," *Journal of Physics and Chemistry of Solids*, vol. 19, no. 1, pp. 35–50, 1961.

[51] C. Wagner, "Theorie der alterung von niederschlägen durch umlösen (ostwald-reifung)," *Zeitschrift für Elektrochemie, Berichte der Bunsengesellschaft für physikalische Chemie*, vol. 65, no. 7-8, pp. 581–591, 1961.

[52] G. K. Batchelor, *An introduction to fluid mechanics*. Cambridge University Press, 1967.

Glossary

List of Acronyms

AM	Applied Mathematics
AP	Apparent Porosity
BSG	Bulk specific gravity
EEMCS	Electrical Engineering, Mathematics and Computer Science
GLS	Galerkin Least-Squares
ODE	Ordinary Differential Equation
PDE	Partial Differential Equation
SEM	Scanning electron microscopy
SG	Specific Gravity
SUPG	Streamline-Upwind/Petrov-Galerkin
TP	True Porosity
WA	Water Absorption